Local and distortional buckling behaviour of aluminium alloy back-to-back channels with web holes under axial compression

Zhiyuan Fang[a], Krishanu Roy[a*], Boshan Chen[a], Zhengxin Xie[a], James B.P. Lim[a]

a Department of Civil and Environmental Engineering, The University of Auckland, New Zealand

Abstract: Aluminium alloy back-to-back channels are becoming popular in building structures. These back-to-back channels often include web holes for installation of services. No previous research, however, is available in the literature for compressive behaviour of aluminium alloy back-to-back channels with web holes. This paper presents an experimental and numerical investigation on the behaviour of screw fastened back-to-back built-up aluminium alloy stub and short columns with web holes under axial compression. Fourteen tests were conducted in total, the results of all are reported in this paper. Prior to compression tests, tensile tests were conducted to determine the material properties of test specimens and initial geometric imperfections were also measured using a laser scanner. A non-linear finite element (FE) model was then developed, and the results were compared against the experiment results showing a good match in terms of both the axial strength and failure modes. Based on 720 FE models, a comprehensive parametric study was conducted to investigate the effects of hole size, screw spacing, section thickness, column length and modified slenderness on structural behaviour of back-to-back built-up aluminium alloy channel columns. Furthermore, the performance of current design guidelines by Australian/New Zealand Standards (AS/NZS) and the American Iron and Steel Institute (AISI) standards was assessed by comparing the axial strengths obtained from the experiments and FEA. It is shown that the AISI & AS/NZS (4600:2018) are conservative by 10% on average, when compared against the test results. Parametric study results were used to propose the axial strength reduction factor equations for aluminium alloy back-to-back channels, and thereafter a reliability analysis was performed.

The results of reliability analysis showed that the proposed equations could closely predict the reduced axial strength of aluminium alloy back-to-back channels with web holes.

Keywords: Axial compression test, finite element analysis, aluminium alloy, web hole, built-up section

1 Introduction

In recent years, the use of aluminium alloy structural members has seen a significant increase due to its attractive attributes such as excellent corrosion resistance, high strength to weight ratio, ease of maintenance, convenience for transportation and recyclability. In order to achieve higher strengths and better resistance against different buckling failures, these channels can be connected back-to-back, with the help of intermediate screw fasteners [1]. On another note, the channels often include web holes for installation of services. Such web holes, however, reduce the axial strength of channel sections [2-7]. This paper investigates the local and distortional buckling behaviour of aluminium alloy back-to-back channels (BTB) with web holes (see Fig. 1). A total of 14 new experimental tests and 720 finite element analyses (FEA) results are reported in this paper.

Design rules for aluminium single channels are available in the Aluminium Design Manual (ADM) [8], Australian/New Zealand Standards (AS/NZS) [9-10] and Eurocode 9 (EC9) [11]. However, the design recommendations for axial capacity of aluminium BTB channels are not included in these standards. Based on the guidelines of American Iron and Steel Institute (AISI) [12] and Australian and New Zealand Standards (AS/NZS) [13], the axial strength of built-up columns with web holes can be calculated by introducing modified slenderness and reduced section properties. However, these design rules are for carbon steel instead of aluminium alloy, but the calculation results from Roy et al. [14] have shown that the carbon steel design rules of AISI [12] and AS/NZS [13] could be used to calculate the axial strength of aluminium BTB channels accurately. This paper has therefore used the design rules of carbon steel built-up channels in accordance with the AISI [12] and AS/NZS [13], while calculating the axial strength of aluminium alloy BTB channels with web holes.

In terms of the cold-formed carbon steel built-up section columns, Wang et al. [15] investigated the structural performance of back-to-back channels with web holes under axial compression. Similarly, Stone and LaBoube [16] studied the effects of web holes on the axial strength of double-limb built-up columns. Roy et al. [17-21] carried out similar research where experimental tests and FEA of different cross sections of built-up columns were performed (Figs. 2(a) and 3(b)). Fratamico et al. [22-23] conducted experimental tests on the buckling behaviour of cold-formed steel (CFS) BTB channels. Moreover, Dabaon et al. [24-25] and Anbarasu et al. [26-27] conducted experimental tests and numerical simulation on the axial compressive behaviour of CFS built-up channels (Fig.2(c)). Most recently, Roy et al. [28] studied the axial compressive behavior of face-to-face built-up CFS channels (Fig.2(d)). In terms of CFS built-up sections with stiffeners, Zhang and Young [29-31] studied the structural performance of built-up CFS channels with stiffeners subjected to axial compression (Figs.2(e) and 2(f)).

Stainless steel built-up columns are also popular among engineering applications [32]. Current design guidelines in accordance with the AS/NZS [33], AISI [12], and ASCE [34] provide design recommendations for calculating the axial strength of stainless steel built-up columns. Yuan et al. [35], Roy et al. [36-39] and Dobric et al. [40-41] carried out experimental and numerical studies to investigate the axial compressive behaviour of cold-formed stainless steel built-up channels. Besides, Kechidi et al. [42-43] studied the effects of screws on the structural behaviour of cold-formed stainless steel built-up channels under axial compression.

In terms of aluminium alloy sections, most research studies available in the literature cover only single sections. Feng et al. [44-48] studied the mechanical behaviour of perforated aluminium alloy single channel columns and found that the current design guidelines [8-11] are not reliable to predict the axial strength of such aluminium alloy single channels. Pham et

al. [49-51] and Mazzolani et al. [52-53] conducted investigations on the buckling behaviour of aluminium alloy channels subjected to axial compression. For calculation method, Young et al. [54-56] applied the Continuous Strength Method (CSM) on the structural behaviour of aluminium alloy channels, and it was concluded that CSM could well predict the axial strength of such members. For aluminium BTB channels, Roy et al. [14] studied the local and distortional buckling behaviour of aluminium BTB channels, however the built-up channels investigated by Roy et al. [14] were non-perforated and it is worth noting that not even a single study is available in the literature which investigated the buckling behaviour of aluminium alloy BTB channel sections with web openings under axial compression.

This paper reports the analysis of 14 new experimental tests on the buckling behaviour of aluminium alloy BTB channels with web holes. Prior to experimental tests, the material properties of the investigated specimens were obtained from the tensile coupon tests, and the initial geometric imperfections were measured by a laser scanner. A non-linear finite element (FE) model, which incorporated both material non-linearities and initial geometric imperfections, was then developed and validated against the test results. The current design rules of AISI [12] and AS/NZS [13] were assessed by comparing the results of tests and FEA. A comprehensive parametric study based on 720 FE models was then carried out to investigate the effects of hole size, screw spacing, section thickness, column length and modified slenderness on the axial strength of such columns. Finally, design equations in the form of axial strength reduction factors were proposed for aluminium alloy BTB channels with web holes. A reliability was then conducted, which showed that the proposed reduction factor equations could closely predict the axial strength of aluminium alloy BTB channels with web holes.

2 Experimental tests

2.1 Test specimens

Axial compression tests of 14 aluminium BTB channels were conducted. Fig.1 and Table 1 show the cross-sectional details of test specimens (with two lengths: stub (300 mm) and short (500 mm) columns). The spacing of fasteners and ratios of hole diameters to overall web depth were designed to investigate the effects of varying screw spacing and web hole size on columns with varying length, and the design of screw spacing was based on the clause C4.5 of AISI [57].

The specimens were labelled to cover the related details (Fig.3). For example, the label "BU240-t1.98-L300-S50-A0.6" can be interpreted as follows:

- The number "240" refers to the nominal dimension of the web depth in millimetres i.e., d=240 mm.
- "t1.98" represents section thickness in millimetres i.e., t =1.98 mm.
- "L300" refers to the column length in millimetres i.e., L=300 mm.
- "S50" refers to the screw spacing in millimetres i.e., S =50 mm.
- "A0.6" represents the ratio of hole diameter to overall web depth i.e., a/d=0.6.

2.2 Tensile tests

5052-H32 aluminium alloy was used for the investigated specimens in this paper. The detailed material properties were obtained from the tensile coupon tests. The tensile coupons were cut from the centre of the web plate in the longitudinal direction of the untested specimens. Based on the requirements of British Standard for Testing and Materials [58], the detailed dimensions of coupons were prepared as reported in Table 2. When the tensile coupons were tested in an Instron testing machine (Fig.4) having 50kN- capacity, the tensile strain of

the coupons was obtained from a calibrated extensometer. Fig.5 shows the full stress-stain curve of the specimens, and Table 3 listed the detailed material properties of the tested coupons.

2.3 Test setup for compression tests

The aluminium BTB channels were tested in the testing machines under pin-pin support boundary conditions, and an external load cell was used to apply the load through the centre of gravity (CG) of the section. The lubricating oil was applied whenever the test was conducted in the bolt connector which could reduce the effect of friction from the bolt connector on the axial strength. In Fig.6 and Fig.7 are shown the test setup and the pin support. A displacement control with a constant loading rate at 0.02 mm/s was used in the column tests. The displacement was recorded by using the three linear variable differential transformers (LVDTs). LVDT-1 was used to record the axial shortening, and LVDT-2 and 3 were placed at mid-height of the specimens to record the lateral displacement.

2.4 Initial geometric imperfections

A laser scanner was used to measure the initial geometric imperfections of the investigated aluminium BTB channels along six longitudinal lines on the specimens (Fig.8 and Fig.9), and the imperfection data was recorded at every 0.1mm.

The imperfection data of a typical profile BU240-t1.98-L500-S100-A0.2 is shown in Fig.10, and the maximum local, distortional, and global imperfection magnitudes of the specimens are listed in Table 4. Local initial imperfection was determined based on the readings recorded along the lines W-1 and W-2 and W-3, as shown in Fig.10(a). Based on the average value of the recorded readings along the line W-2 at the mid height of the columns, the global imperfection was calculated (Fig.10(b)). In Fig.10(c), the distortional imperfection on the flange was calculated based on the data recorded in lines F-1 and F-2. The magnitudes of these imperfections were included in the FE modelling described in section 3.6 of this paper.

146 *2.5 Experimental results*

147 In total, 14 compression tests were conducted, and the test results are listed in Table 1.
148 As can be seen from Table 1, local and distortional buckling modes were observed for all
149 specimens including stub and short columns. Fig.11 shows the failure modes of some test
150 specimens. Fig.12 plots the axial load versus mid-height lateral displacement graphs for
151 BU240-t1.98-L300-S50-A0.2, BU240-t1.98-L500-S100-A0.2, BU240-t1.98-L300-S50-A0.2
152 and BU240-t1.98-L500-S400-A0.2.

153 The axial shortening versus loading behaviour is shown in Fig.13. Prior to the plastic
154 stage, the load-axial shortening behaviour was almost linear up to a load at 105 kN, which is
155 approximately 89.98% of the ultimate failure load (116.69kN) of BU240-t1.98-L300-S50-A0.2
156 specimen. When the tested specimen reached the plastic stage, nonlinear behaviour was
157 observed. Similar observation was noticed for the cases of other test specimens.

158 The effects of hole size on axial strength of aluminium alloy built-up columns were
159 studied and the results are reported in Table 1 and in Fig.14. As shown in Fig.14(a), the axial
160 strength of stub columns (BU240-t1.98-L300-S50) was decreased by 2.93% on average when
161 the *a/h* ratio was changed from 0 to 0.2. Upon tripling the *a/h* ratio from 0.2 to 0.6, an average
162 reduction of 7.93% in axial strength was observed for stub columns (BU240-t1.98-L300-S50).
163 From Fig.14(c), it can be seen that the average strength of the short columns (BU240-t1.98-
164 L500-S100) was increased by 1.40%, when the *a/h* ratio was increased from 0 to 0.2.
165 Meanwhile, the reduction in axial strength was not prominent (by 0.49%) when *a/h* ratio was
166 increased from 0.2 to 0.6 for short columns (BU240-t1.98-L500-S100).

167 The local and distortional buckling failures were observed for BU240-t1.98-L300-S50-
168 A0.2, where two single channels were connected by five screw fasteners having screw spacing
169 of 50mm. The aluminium BTB perforated channels remained integral at failure, and the

localized deformation near the end of the columns was observed at ultimate load, as shown in Fig.11.

3 Numerical simulations

3.1 General

A nonlinear FE model was developed using ABAQUS [59] software to simulate the axial compressive behaviour of aluminium BTB channels with web holes. The FE model included the nonlinear material properties, initial geometric imperfections and residual stresses.

3.2 Modelling of material properties

The obtained material properties from tensile coupon tests were incorporated into the FE models, and the engineering material curve was converted into a true material curve by using the equations below:

$$\sigma_{true} = \sigma(1+\varepsilon) \quad (1)$$

$$\varepsilon_{true(pl)} = ln(1+\varepsilon) - \frac{\sigma_{true}}{E} \quad (2)$$

Where, σ_{true} and $\varepsilon_{\text{true(pl)}}$ are the true stress and strain, respectively. σ and ε are the engineering stress and strain, respectively. E is the young's modulus.

3.3 FE meshing

S4R shell elements and rigid quadrilateral shell elements (R3D4) were used to model the aluminium BTB channels and loading plates, respectively. Mesh sizes of 5 mm × 5 mm and 10 mm × 10 mm were used for modelling the channel sections and endplates, respectively. Fig.15(a) shows a typical FE mesh for BU240-t1.98-L300-S200-A0.4.

3.4 Boundary conditions

The aluminium BTB channels with web holes were pin ended columns. As shown in Fig.15(a), the displacements and rotations were applied through the reference points defined at the end plates. The reference points were set at the CG of the cross sections. For the loading

applied to the top plate, x- and y- translations were restrained, while z- translation was set as free. Meanwhile, all translations at the bottom plate were restrained through the reference point. It should be noted that both the top and bottom plates were set as free to rotate along the minor axis. Screws were simulated using the MPC beam connector elements.

3.5 Contact modelling

"Surface to surface" contact was used to model the interaction between the webs of two single channels and between the base plates and channels. The normal behaviour of the surface was defined as "hard", indicating that the penetration between the two surfaces was not allowed. A fixed value of 0.5 was used was the friction co-efficient in the FE model developed using ABAQUS [59]. The value of the friction co-efficient was based on the calibration of the FEA model and its comparison against the test results using different friction coefficient values. The contact between two surfaces can play an important role in load carrying capacity [60-62], and therefore it is important to consider in the effect of friction between two surfaces as also reported by a number of previously published papers [63-70].

3.6 Initial geometric imperfections and residual stresses

Eigenvalue analysis was conducted to determine the contours of local and distortional imperfections, as shown in Fig.15(b). The local and distortional buckling modes were modelled based on the lowest buckling mode obtained from the eigenvalue analysis. The imperfections used in the modelling of aluminium BTB channels with web holes, were scaled to the values given in the experimental program (Table 4). The same technique was also applied by Roy et al. [14] to model the initial geometric imperfection of non-perforated aluminium alloy BTB channel columns.

The residual stresses and corner enhancements in the corner portion of the channels were modeled in the FEA, as per the guidelines proposed by Moen et al. [71]. This method was also employed by Fang et al. [72-73].

3.7 FE validation

In Table 1, the axial strengths obtained from the experimental tests are compared with the FEA strengths. Compared to the experimental results, FE results were close in terms of both the axial strengths and failure modes. Fig.16 shows the deformed shapes of investigated columns obtained from the FEA, showing good agreement with the failure modes obtained from the experiments. Fig.17 plots the load-axial shortening behaviour obtained from the FEA and experiments. In fact, the initial stiffness of the experimental curves is a little lesser than that of FEA curves. This might be a consequence of the gap between the channel and top/bottom supports, during conducting the tests in the laboratory. The mean values of the ratio of test to FEA results (P_{EXP}/P_{FEA}) are 1.03 and 1.02 with the corresponding COVs of 0.01 and 0.02, respectively for stub and short columns. Overall, the FE model showed very good agreements with the experimental results.

4 Parametric study

A parametric investigation based on 720 FE models was carried out to study the effects of different parameters on the axial strength of aluminium BTB channels with web holes. The range of parameters include modified slenderness covering stub and columns, number of screw fasteners (2,3 and 5 number of screws), section thickness from 0.5 to 2.9mm, and column length from 300 to 800mm.

Based on the previous research studies [14, 72-73], it was found that the axial strength (P) and the axial strength reduction factor (R) of aluminium BTB channels with web holes

239 depend mainly on the ratio of hole diameter to web depth (*a/h*), screw spacing (number of
240 screws), section thickness (*t*), column length (*L*) and modified slenderness ($(KL/r)_m$).

241 *4.1 Parametric study on the axial strength (P) of aluminium BTB channels*

242 *4.1.1 Effect of a/h ratio on the axial strength (P)*

243 The effect of *a/h* ratio on the axial strength of aluminium BTB channels was studied.
244 From Fig.18(a), it can be seen that when the ratio *a/h* was increased, the axial strength of
245 aluminium BTB channels was generally decreased. When the *a/h* ratio was increased from 0
246 to 0.8, the average axial strengths of aluminium BTB channels were decreased by 2.37%,
247 2.82%, 4.82% and 17.25%, respectively for each increment of *a/h* ratio by 0.02.

248 *4.1.2 Effect of screw number (n) on the axial strength (P)*

249 Fig.18(b) presents the effect of screw number (*n*) on the axial strength of built-up
250 columns. When the screw numbers (*n*) were increased from 2 to 5, the average strength of all
251 sections increased slightly by 2.68%. It should be noted that the average strength of plain
252 sections with 5 screws are higher than that of plain sections with 2 screws (by around 2.27%
253 for nonperforated sections and by 2.78% for perforated sections).

254 *4.1.3 Effect of section thickness (t) on the axial strength (P)*

255 From parametric study results, it was observed that the section thickness (*t*) significantly
256 affects the axial strength of aluminium BTB channels with web holes, as also shown in Table
257 5 and Fig.18(c). With the increase of *t* from 0.5mm to 2.9mm, the average axial strength of
258 aluminium BTB plain channels increased from 12.04kN to 180.52kN, and the values for
259 channels with web holes changed from 11.23kN to 164.65kN.

260 *4.1.4 Effect of column length (L) on the axial strength (P)*

261 It can be seen from Fig.18(d) that when the column length changed from 300mm to
262 800mm, the local and distortional buckling dominate the failure modes. The average strength

of all investigated sections was reduced by 12.61%, and 12.78%, respectively for plain and perforated built-up sections, when the column lengths were increased from 300mm to 800mm.

4.1.5 Effect of modified slenderness ($(KL/r)_m$) on the axial strength (P)

As shown in Table 5 and in Fig.18(e), modified slenderness $(KL/r)_m$ also affects the axial strength of aluminium BTB channels. The results from Table 5 and Fig.18(e) demonstrate the reduction in axial strengths by 14.96% and 10.10% on average for plain and perforated built-up sections, respectively, when the modified slenderness ($(KL/r)_m$) ratio was increased from 16.51 to 62.73.

4.2 Parametric study on the strength reduction factor (R)

4.2.1 Effect of a/h ratio on the strength reduction factor (R)

Fig.19(a) shows a downward trend of axial strength reduction factor with the increase in *a*/*h* ratio from 0.2 to 0.8. From Table 6, it can be seen that the reduction factors for sections with varied column lengths and number of screws are similar, i.e., 0.98 for sections with the ratio at 0.2; 0.97 for sections with the ratio at 0.4; 0.95 for sections with the ratio at 0.6; 0.85 for sections with the ratio at 0.8.

4.2.2 Effect of screw number (n) on the strength reduction factor (R)

Fig.19(b) shows the effect of screw number (*n*) on the strength reduction factor (*R*). There is very little difference of the average strength reduction factors for sections with varied screw numbers, the value being 0.93. There is not much difference of the strength reduction factor (*R*) from different screw numbers, and thus the effect of screw number (*n*) on the strength reduction factor (*R*) is not so important.

4.2.3 Effect of section thickness (t) on the strength reduction factor (R)

The effect of section thickness (*t*) on the strength reduction factor (*R*) was also studied in the parametric investigation. From Fig.19(c), it can be seen that when the value of *R* was varied

from 0.72 to 0.99, the average *R* values for each group of section thickness remained constant at 0.94.

4.2.4 Effect of column length (L)and modified slenderness ($(KL/r)_m$) on the strength reduction factor (R)

Figs.19(d) and (e) show that the strength reduction factor (*R*) varied from 0.72 to 0.99, when the column length (*L*) was changed from 300mm to 800mm. For section with column length over 700mm (modified slenderness over 39.01), the COVs of the *R* value are lower than those of the other lengths.

5 Design guidelines for axial strength of aluminium BTB channels

No design guideline is available in the existing standards for axial strengths of aluminium BTB channels with web holes. However, there are design guidelines mentioned in the AISI [12] and AS/NZS [13] for carbon steel built-up columns with web holes. Therefore, the related design rules available in the AISI [12] and AS/NZS [13] for such carbon steel columns with web holes were used in this study. Besides, it should be noted that the aluminium alloy does not have a distinct yield stress, and thus the axial strengths of aluminium BTB channels were determined from the design formulae of CFS perforated channels by replacing the yield stress of carbon steel with the 0.2% proof stress of aluminium alloy material.

5.1 Design rules for CFS back-to-back plain channels

The un-factored design strengths of cold-formed carbon steel built-up columns in accordance with the AISI [12] and AS/NZS [13] standards can be determined using Equation (3) below:

$$P_{\mathrm{AISI\&AS/NZS}} = A_e F_n \tag{3}$$

The critical elastic buckling stress (F_n) can be determined using Equations (4)-(5) as follows:

311 $$\text{For } \lambda_c \leq 1.5,\ F_n = \left(0.658^{\lambda_c^2}\right) F_y \quad (4)$$

312 $$\text{For } \lambda_c > 1.5,\ F_n = \left(\frac{0.877}{\lambda_c^2}\right) F_y \quad (5)$$

313 Where non-dimensional critical slenderness (λ_c) was determined using Equation (6):

314 $$\lambda_c = \sqrt{\frac{f_y}{f_{oc}}} \quad (6)$$

315 Where, f_y is yield stress and f_{oc} is the least of elastic flexural, torsional, and flexural-torsional
316 buckling stress calculated in accordance with the AISI [12] and AS/NZS [13].

317 Modified slenderness ratio was calculated as per equation 7, and was used in all the
318 design calculations to determine the axial strength of back-to-back built-up columns

319 $$\text{For } \left(\frac{a}{r_i}\right) \leq 0.5\left(\frac{KL}{r}\right)_o,\ \left(\frac{KL}{r}\right)_m = \sqrt{\left(\frac{KL}{r}\right)_o^2 + \left(\frac{a}{r_i}\right)^2} \quad (7)$$

320 Where, $(KL/r)_o$ is the overall slenderness ratio; a is the intermediate fastener spacing; and r_i is
321 the minimum radius of gyration of full unreduced cross-sectional area of an individual shape
322 in a built-up member.

323 *5.2 Design rules for CFS back-to-back channels with web holes*

324 The axial strength of CFS back-to-back channels with web holes can be calculated by
325 following the calculation procedure of section 5.1. The reduction due to the web holes should
326 be considered in the calculation of section properties.

327 *5.3 Comparison of design strengths with test and FE strengths*

328 Experimental and FEA strengths were compared with the calculated design strengths in
329 accordance with the AISI [12] and AS/NZS [13]. From Table 7 and Fig.20, it can be concluded
330 that the design strengths calculated from the AISI [12] and AS/NZS [13] were conservative by
331 5%-30%, when compared to the experimental results.

6 Proposed design equations

6.1 Design equations for aluminium BTB channels with web holes

As mentioned previously, the validated FE models could predict the reduced axial strength of aluminium BTB channels with web holes more accurately compared to the predictions of current design standards. Therefore, the design equations on axial strength reduction factors of aluminium BTB channels with web holes were proposed based on the validated FE models. The limits for the proposed equations are $h/L \leq 0.8$, $h/t \leq 480$ and $a/h \leq 0.8$.

Design equations in relation to the *a/h* ratio were developed for axial strength reduction factors (R_{prop}) based on the regression analysis method employed by Fang et al. [73-76], Roy.et al. [78-80] and Chen et al. [81-83]. The proposed design equations for sections with one circular web hole are given below:

For stub columns ($(KL/r)_m \leq 29.05$),

$$R_{prop} = 1 + 0.449\left(\frac{a}{h}\right)^{-0.676} \leq 1 \tag{8}$$

For stub columns ($29.05 < (KL/r)_m \leq 62.73$),

$$R_{prop} = 1 + 0.506\left(\frac{a}{h}\right)^{-0.610} \leq 1 \tag{9}$$

As for prediction accuracy of the proposed equations, Table 8 shows that the proposed reduction factor R_{prop} is very close to the experimental results, which confirms the accuracy of the proposed design equations.

6.2 Reliability analysis

Using the method mentioned in both Fang et al. [72-76] and Hsiao et al. [84], a reliability analysis was carried out to evaluate the accuracy of proposed design equations. As mentioned

in AISI S100-16 [12], any proposed design equation can be considered reliable when the reliability index (β) is greater than or equal to the target reliability index of 2.50. In Table 9, the values of β for aluminium BTB stub and short columns with web holes are over 2.50. This indicates that the proposed design equations can be used to determine the reduced axial capacity of aluminium BTB channels with web holes with high degree of precisions.

7 Conclusions

The paper reported a detailed experimental study on aluminium back-to-back channels with web holes under axial compression. The results from a total of 14 new tests are reported herein. Prior to compression tests, the material properties of test specimens were obtained from the tensile coupon tests, and the initial geometric imperfections were measured by using a laser scanner. The axial strengths, failure modes, load-axial shortening, and load-lateral displacement behaviours were discussed. In the experimental study, the effects of hole size, screw spacing, section thickness, column length and modified slenderness were also investigated.

A non-linear finite element (FE) model, which incorporated material non-linearities, initial geometric imperfections and residual stresses, was then developed and validated against the test results. Furthermore, a comprehensive parametric study based on 720 FE models was carried out to investigate the effects of different parameters including hole size, screw spacing, section thickness, column length and modified slenderness on the axial strength of aluminium BTB channels with web holes. The results from the parametric study show that the section thickness (t) affect the axial strength of such aluminium built-up columns significantly. With the increase of t from 0.5mm to 2.9mm, the average axial strength of aluminium BTB plain channels were increased from 12.04kN to 180.52kN, and the values for perforated channels changed from 11.23kN to 164.65kN. However, the effect of modified slenderness on axial

strength of stub and short columns was not noticeable. The axial strengths of the investigated sections were reduced by 14.96% and 10.10% on average for plain sections and perforated sections, respectively, when the modified slenderness ($(KL/r)_m$) was increased from 16.51 to 62.73. Screw numbers had a limited impact on the axial strength of perforated aluminium alloy BTB channels. The axial strengths of columns were increased by 2.27% and 2.78% on average for plain sections and perforated sections, respectively, with the screw numbers changed from 2 to 5.

The design strengths obtained from the tests and FEA were compared with the design strengths calculated in accordance with the Australian/New Zealand Standards (AS/NZS), and American Iron and Steel Institute (AISI) standards. The comparison results showed that the AISI and AS/NZS standards are conservative by 10% on average for perforated aluminium alloy BTB columns failed mainly by local and distortional buckling.

Finally, design recommendations in the form of axial strength reduction factors have been proposed for the aluminium BTB channels with web holes. Reliability analysis was also carried out to demonstrate the reliability of the proposed design equations while predicting the reduced axial strength of aluminium BTB channels with web holes.

Acknowledgements

We sincerely thank the contributions of "Structure's test hall" and "Data visualization Lab" of The University of Auckland for providing us good facilities while performing the experimental tests and numerical simulation.

References

[1] K. Roy, H. H. Lau, Z.Y. Fang, R. Masood, T.C.H Ting, J.B.P. Lim, V.C.C. Lee, Effects of corrosion on strength of the self-drilling screw connections in cold-formed steel structures-Experiments and finite element modeling. Struct. (2021) (under review).

[2] Yu, N., Kim, B., Li, L., Hong, W., & Yuan, W. (2020). Distortional buckling of perforated cold-formed steel beams subject to uniformly distributed transverse loads. Thin-Walled Structures, 148, 106569.

[3] Yu, N., Kim, B., Huang, X., Yuan, W., Ye, R., Wu, L., & Le, J. (2021). Analytical solution for flange/web distortional buckling of cold-formed steel beams with circular web perforations. Mechanics of Advanced Materials and Structures, 1–11.

[4] Yu, N., Kim, B., Yuan, W., Li, L., & Yu, F. (2019). An analytical solution of distortional buckling resistance of cold-formed steel channel-section beams with web openings. Thin-Walled Structures, 135, 446–452.

[5] Yuan, W., Yu, N., & Li, L. (2017). Distortional buckling of perforated cold-formed steel channel-section beams with circular holes in web. International Journal of Mechanical Sciences, 126, 255–260.

[6] Moen, C. D., & Schafer, B. W. (2009). Elastic buckling of cold-formed steel columns and beams with holes. Engineering Structures, 31(12), 2812–2824.

[7] Moen, C. D., & Schafer, B. W. (2011). Direct Strength Method for Design of Cold-Formed Steel Columns with Holes. Journal of Structural Engineering, 137(5), 559–570.

[8] The Aluminium Association, Aluminium Design Manual (ADM). The Aluminium Association, Washington, D.C., USA, 2015.

[9] Australian/New Zealand Standard (AS/NZS). Aluminium Structures Part 1: Limit State Design. AS/NZS 1664.1: 1997, Sydney, Australia, 1997.

[10] Australian/New Zealand Standard (AS/NZS), Aluminium Structures Part 2: Allowable Stress Design, AS/NZS 1664.2: 1997, Sydney, Australia, 1997.

[11] Eurocode 9 (EC9), Design of Aluminium Structures - Part 1-1: General Structural Rules, European Committee for Standardization, EN 1999-1-1:2007, CEN, Brussels, Belgium, 2007.

[12] American Iron and Steel Institute (AISI). North American Specification for the Design of Cold-formed Steel Structural Members AISI D100-17E; 2017.

[13] Australia/New Zealand Standard (AS/NZS). Cold-Formed Steel Structures, AS/NZS 4600:2018. Standards Australia/ Standards New Zealand; 2018.

[14] K. Roy, B.S. Chen, Z.Y. Fang, A. Uzzaman, X. Chen, J.B.P. Lim, Local and distortional buckling behaviour of back-to-back built-up aluminium alloy channel section columns, Thin-Walled Struct. 163(1) (2021).

[15] C.G. Wang, Q.L. Guo, Z.G. Zhang, Y.T. Guo, Experimental and numerical investigation of perforated cold-formed steel built-up I-section columns with web stiffeners and complex edge stiffeners, Adv. Struc. Eng. 22 (2019) 2205-2221.

[16] T. A. Stone, R. A. LaBoube, Behavior of cold-formed steel built-up I-sections, Thin-Walled Struct. 43(2005) 1805-1817.

[17] Chen, B., Roy, K., Uzzaman, A., Raftery, G., & Lim, J. B. P. (2020). Axial strength of back-to-back cold-formed steel channels with edge-stiffened holes, un-stiffened holes and plain webs. Journal of Constructional Steel Research, 174, 106313.

[18] K. Roy, T.C.H. Ting, H.H. Lau, J.B.P. Lim, Effect of thickness on the behaviour of axially loaded back-to-back cold-formed steel built-up channel sections-experimental and numerical investigation, Struct. 16 (2018) 327-346.

[19] T.C.H. Ting, K. Roy, H.H. Lau, J.B.P. Lim, Effect of screw spacing on behavior of axially loaded back-to-back cold-formed steel built-up channel sections, Adv. Struct. Eng. 21 (2018) 474-487.

[20] K. Roy, T.C.H. Ting, H.H. Lau, J.B.P. Lim, Nonlinear behavior of back-to-back gapped built-up cold-formed steel channel sections under compression, J. Constr. Steel Res. 147 (2018) 257-276.

[21] K. Roy, H.H. Lau, J.B.P. Lim, Numerical investigations on the axial strength of back-to-back gapped built-up cold-formed stainless steel channels, Adv. Struct. Eng. (2019) 136943321983739.

[22] D.C. Fratamico, S.Torabian, X. Zhao, K.J.R. Rasmussen, B.W. Schafer, Experiments on the global buckling and collapse of built-up cold-formed steel columns, J. Constr. Steel Res. 144 (2018) 65-80.

[23] D.C. Fratamico, S.Torabian, X. Zhao, K.J.R. Rasmussen, B.W. Schafer, Experimental study on the composite action in sheathed and bare built-up cold-formed steel columns, Thin-Walled Struct. 127 (2018) 290-305.

[24] M. Dabaon, E. Ellobody, K. Ramzy, Experimental investigation of built-up cold-formed steel section battened columns, Thin-Walled Struct. 92 (2015) 137-145.

[25] M. Dabaon, E. Ellobody, K. Ramzy, Nonlinear behaviour of built-up cold-formed steel section battened columns, J. Constr. Steel Res. 110 (2015) 16-28.

[26] M. Anbarasu, K. Kanagarasu, S. Sukumar, Investigation on the behaviour and strength of cold-formed steel web stiffened built-up battened columns, Materials and Structures, 12 (2014) 4029-4038.

[27] M. Anbarasu, Behaviour of cold-formed steel built-up battened columns composed of four lipped angles: tests and numerical validation, Adv. Struct. Eng. (2019) 136943321986569.

[28] K. Roy, C. Mohammadjani, J.B.P. Lim, Experimental and numerical investigation into the behaviour of face-to-face built-up cold-formed steel channel sections under compression, Thin-Walled Struct. 134 (2019) 291-309.

[29] J.H. Zhang, B. Young, Finite element analysis and design of cold-formed steel built-up closed section columns with web stiffeners, Thin-Walled Struct. 131 (2018) 223-237.

[30] J.H. Zhang, B. Young, Numerical investigation and design of cold-formed steel built-up open section columns with longitudinal stiffeners, Thin-Walled Struct. 89 (2015) 178-191.

[31] J.H. Zhang, B. Young, Compression tests of cold-formed steel built-up open sections with edge and web stiffeners, Thin-Walled Struct. 52 (2012) 1-11.

[32] B. Young, W. Hartono, Compression tests of stainless steel tubular members, J. Struct. Eng. 128(6) (2002) 754-761.

[33] Australia/New Zealand Standard (AS/NZS). Cold-Formed Steel Structures, AS/NZS 4673-2001. Standards Australia/ Standards New Zealand; 2001.

[34] ASCE, Specification for the Design of Cold-Formed Stainless Steel Structural Members, SEI/ASCE 8-02, American Society of Civil Engineers, New York, 2002 (Standard No. 02-008).

[35] H.X. Yuan, Y.Q. Wang, Y.J. Shi, L. Gardner, Stub column tests on stainless steel built-up sections, Thin-Walled Struct. 83 (2014) 103-114.

[36] K. Roy, H.H. Lau, J.B.P. Lim, Finite element modelling of back-to-back built-up cold-formed stainless-steel lipped channels under axial compression, Steel Compos. Struct. 33 (2019) 37-66.

[37] K. Roy, J.B.P. Lim, Numerical investigation into the buckling behaviour of face-to-face built-up cold-formed stainless steel channel sections under axial compression, Struct. 20 (2019) 42-73.

[38] K. Roy, H.H. Lau, J.B.P. Lim, Numerical investigations on the axial capacity of back-to-back gapped built-up cold-formed stainless steel channels, Adv. Struct. Eng. 22 (10) (2019) 2289-2310.

[39] K. Roy, T.C.H. Ting, H.H. Lau, J.B.P. Lim, Effect of screw spacing into the behaviour of back-to-back cold-formed duplex stainless steel built-up channel sections under compression. International Conference on Engineering Research and Practice for Steel Construction 2018 (ICSC2018). September 5-7 (2018) Hong Kong, China.

[40] J. Dobrić, M. Zlatko, B. Dragan, S. Milan, F. Nenad, Resistance of cold-formed built-up stainless steel columns-Part I: Experiment, J. Constr. Steel Res. 145 (2018) 552-572.

[41] J. Dobrić, P. Marko, M. Zlatko, B. Dragan, S. Milan, Resistance of cold-formed built-up stainless steel columns - Part II: Numerical simulation, J. Constr. Steel Res. 145 (2018) 247-260.

[42] S. Kechidi, D.C. Fratamico, N. Bourahla, J.M. Castro, B.W. Schafer, Numerical study of screw fasteners in built-up CFS chord studs. Ce/papers. 1 (2-3) (2017) 1543-1552.

[43] S. Kechidi, D.C. Fratamico, B.W. Schafer, C.J. Miguel, Simulation of screw connected built-up cold formed steel back-to-back lipped channels under axial compression. Eng. Struct. 206 (2020) 110109.

[44] R. Feng, B. Young, Experimental Investigation of Aluminium Alloy Stub Columns with Circular Openings, J. Struct. Eng. 141(11) (2015) 04015031.

[45] R. Feng, X. Mou, A. Chen, Y. Ma, Tests of aluminium alloy CHS columns with circular openings, Thin-Walled Struct. 109 (2016) 113-131.

[46] R. Feng, W. Sun, C. Shen, J. Zhu, Experimental investigation of aluminium square and rectangular beams with circular perforations, Eng. Struct. 151 (2017) 613-632.

[47] Y. Chen, R. Feng, J. Xu, Flexural behaviour of CFRP strengthened concrete-filled aluminium alloy CHS tubes, Constr Build Mater. 142 (2017) 295-319.

[48] Y. Chen, R. Feng, W. Gong, Flexural behaviour of concrete-filled aluminium alloy circular hollow section tubes, Constr Build Mater. 165 (2018) 173-186.

[49] L.A.T. Huynh, C.H. Pham, K.J.R. Rasmussen, Mechanical properties of cold-rolled aluminium alloy 5052 channel sections. Proceedings of 8th International Conference on Steel and Aluminium Structures, Hong Kong, China 670-684 (2016).

[50] L.A.T. Huynh, C.H. Pham, K.J.R. Rasmussen, Stub column tests and finite element modelling of cold-rolled aluminium alloy 5052 channel sections, in: Proceedings of the Eighth International Conference on Steel and Aluminium Structures, Hong Kong, China 1–14 (2016).

[51] L.A.T. Huynh, C.H. Pham, K.J.R. Rasmussen, Experimental investigation of cold-rolled aluminium alloy 5052 columns subjected to distortional buckling, Lecture Notes in Civil Engineering, 54 (2020) 287-292.

[52] C. Faella, F.M. Mazzolani, V. Piluso, G. Rizzano, Local buckling of aluminium members: testing and classification, J. Struct. Eng. 126 (3) (2000) 353-360.

[53] F.M. Mazzolani, V. Piluso, G. Rizzano, Local buckling of aluminium alloy angles under uniform compression, J. Struct. Eng. 137(2) (2011) 173-184.

[54] M.N. Su, B. Young, L. Gardner, Continuous strength method for aluminium alloy structures, Adv. Mat. Res. 742 (2013) 70-75.

[55] M.N. Su, B. Young, L. Gardner, Testing and design of aluminium alloy cross sections in compression. J. Struct. Eng. 140 (9) (2014) 04014047.

[56] M.N. Su, B. Young, L. Gardner, Assessment of Eurocode 9 slenderness limits for elements in compression. Tubular Structures-Proceedings of the 15th International Symposium on Tubular Structures. May 569-574 (2016) Rio de Janeiro, Brazil.

[57] American Iron and Steel Institute (AISI). North American Specification for the Design of Cold-formed Steel Structural Members AISI S100-07; 2007.

[58] BS EN. Tensile Testing of Metallic Materials Method of Test at Ambient Temperature, British Standards Institution, 2001.

[59] ABAQUS Analysis User's Manual-Version 6.14-2. ABAQUS Inc., USA, 2014.

[60] C. Mathieson, K. Roy, C. G. Clifton, A., Ahmadi, J. B. P. Lim, Failure mechanism and bearing capacity of cold-formed steel trusses with HRC connectors, Eng. Struct. 201 (2019) 109741.

[61] M. A. Dar, N. Subramanian, A. I. Rather, A.R. Dar, J.B.P. Lim, M. Anbarasu, K. Roy, Effect of angle stiffeners on the flexural strength and stiffness of cold-formed steel beams, Steel Compos. Struct. 33 (2) (2019) 225-243.

[62] K. Roy, T. C. H. Ting, H.H. Lau, and J. B. P. Lim, Experimental investigation into the behaviour of back-to-back gapped built-up cold-formed steel channel sections under compression, Wei-Wen Yu International Specialty Conference on Cold-Formed Steel Structures 2018 - Recent Research and Developments in Cold-Formed Steel Design and Construction, Pages 283 - 2972018 Wei-Wen Yu International Specialty Conference on Cold-Formed Steel Structures 2018St. Louis, 7 November 2018 through 8 November 2018.

[63] G.B.G. Ananthi, K. Roy, B.S. Chen, J.B.P. Lim, Testing, simulation and design of back-to-back built-up cold-formed steel unequal angle sections under axial compression, Steel Compos. Struct. 25 (2019) 595-614

[64] K. Roy, H. H. Lau, T. C. H. Ting, B. Chen, J. B. P. Lim, Flexural capacity of gapped built-up cold-formed steel channel sections including web stiffeners, J. Constr. Steel Res. 172 (2020) 106154.

[65] A. Uzzaman, J. B. P. Lim, D. Nash, K. Roy, Cold-formed steel channel sections under end-two-flange loading condition: Design for edge-stiffened holes, unstiffened holes and plain webs, Thin-Walled Struct. 147 (2020) 106532.

[66] A. Uzzaman, J. B. P. Lim, D. Nash, K. Roy, Web crippling behaviour of cold-formed steel channel sections with edge-stiffened and unstiffened circular holes under interior-two-flange loading condition, Thin-Walled Struct. 154, 106813.

[67] K. Roy, H.H. Lau, J. B. P. Lim, Finite element modelling of back-to-back built-up cold-formed stainless-steel lipped channels under axial compression. Steel Compos. Struct. 33 (2019): 37-66.

[68] G.B.G. Ananthi, K. Roy, J.B.P. Lim, Experimental and numerical investigations on axial strength of back-to-back built-up cold-formed steel angle columns, Steel Compos. Struct. 31 (2019) 601-615.

[69] K. Roy, H. H. Lau, T. C. H. Ting, R. Masood, A. Kumar, J. B. P. Lim, Experiments and finite element modelling of screw pattern of self-drilling screw connections for high strength cold-formed steel, Thin-Walled Struct. 145 (2019) 106393.

[70] B.S. Chen, K. Roy, A. Uzzaman, G. M. Raftery, J. B. P. Lim, Parametric study and simplified design equations for cold-formed steel channels with edge-stiffened holes under axial compression, J. Constr. Steel Res. 172 (2020) 106161.

[71] C.D. Moen, T. Igusa, B.W. Schafer, Prediction of residual stresses and strains in cold-formed steel members, Thin-Walled Struct. 46(11) (2008) 1274-1289.

[72] Z.Y. Fang, K. Roy, J. Mares, C.-W. Sham, B.S. Chen, J.B.P. Lim, Deep learning-based axial capacity prediction for cold-formed steel channel sections using Deep Belief Network, Struct. 33 (2021) 2792–2802.

[73] Z.Y. Fang, K. Roy, B.S. Chen, C.-W. Sham, I. Hajirasouliha, J.B.P. Lim, Deep learning-based procedure for structural design of cold-formed steel channel sections with edge-stiffened and un-stiffened holes under axial compression, Thin-Walled Struct. (2021).

[74] Z.Y. Fang, K. Roy, Q. Ma, A. Uzzaman, J.B.P. Lim, Application of deep learning method in web crippling strength prediction of cold-formed stainless steel channel sections under end-two-flange loading, Struct. 33 (2021) 2903-2942.

[75] Z.Y. Fang, K. Roy, Y. Chi, B. Chen, J. B.P. Lim, Finite element analysis and proposed design rules for cold-formed stainless steel channels with web holes under end-one-flange loading, Struct. (2021) 2876-2899.

[76] Z.Y. Fang, K. Roy, A. Uzzaman, J. B.P. Lim, Numerical simulation and proposed design rules of cold-formed stainless steel channels with web holes under interior-one-flange loading, Eng. Struct. 2021, accepted.

[77] Y.H. Chi, K. Roy, B.S. Chen, Z.Y. Fang, A. Uzzaman, G.B.G. Ananthi, J.B.P. Lim, Effect of web hole spacing on axial capacity of back-to-back cold-formed steel channels with edge-stiffened holes, Steel Compos. Struct. 40 (2) (2021) 287-305

[78] K. Roy, B.S. Chen, Z.Y. Fang, A. Uzzaman, J.B.P. Lim, Axial capacity of back-to-back built-up aluminium alloy channel section columns, ASCE J. Struct. Eng. 2021 (Accepted)

[79] K. Roy, H. H. Lau, Z.Y. Fang, A. M. M. Ahmed, J. B.P. Lim, Axial capacity of back-to-back built-up cold-formed stainless steel unlipped channels-Numerical investigation and parametric study, Steel Compos. Struct. 40(5) (2021) 761-780.

[80] K. Roy, H. H. Lau, Z.Y. Fang, A. M. M. Ahmed, J. B.P. Lim, Axial capacity of back-to-back built-up cold-formed stainless steel unlipped channels-Numerical investigation and parametric study, Steel Compos. Struct. 40(5) (2021) 761-780.

[81] B.S. Chen, K. Roy, Z.Y. Fang, A. Uzzaman, G. Raftery, J. B. P. Lim, Moment capacity of back-to-back cold-formed steel channels with edge-stiffened holes, un-stiffened holes, and plain webs, Eng. Struct. 235 (2021) 112042.

[82] B.S. Chen, K. Roy, Z.Y. Fang, A. Uzzaman, Y.H. Chi, J.B.P. Lim, Web crippling capacity of fastened cold-formed steel channels with edge-stiffened web holes, un-stiffened web holes and plain webs under two-flange loading, Thin-Walled Struct, 163 (2021) 107666.

[83] B.S. Chen, K. Roy, Z.Y. Fang, A. Uzzaman, C. H. Pham, G. Raftery, J. B.P. Lim. Shear behaviour and design cold-formed steel channels with edge -stiffened hole, un-stiffened hole, and plain web, ASCE J. Struct. Eng. (2021) (Accepted).

[84] L. Hsiao, W. Yu, T.V. Galambos, Load and resistance factor design of cold formed steel, calibration of the AISI design provisions, Ninth Progress Report, Civil Engineering Study 88-2, University of Missouri-Rolla, Rolla, Missouri, U.S.A., February 1988.

Notations

a	Screw spacing from the AISI & AS/NZS (4600:2018);
A’	Total length of the web;
A_{eff}	Effective area of the section;
A_{g}	Gross cross-sectional area;
B’	Total length of the flange;
CFS	Cold-formed steel;
COV	Coefficient of variation;
E	Young’s modulus of elasticity;
f_c	Stress from the ADM;
f_{oc}	Least of the elastic flexural, torsional, and flexural torsional buckling stress;
f_{cy}	Compressive yield strength from the ADM;
f_e	Least of the elastic flexural, torsional, and flexural torsional buckling stress;
F_y	Yield stress of the cold-formed steel;
FEA	Finite element analysis;
$(KL/r)_{\text{ms}}$	Modified slenderness;
$(KL/r)_{\text{o}}$	Overall Slenderness from the AISI & AS/NZS (4600:2018);
L	Total length of the back-to-back built-up aluminium alloy channel sections;
LVDT	Linear variable displacement transducers;
n	Screw number;
$P_{\text{AISI\&AS/NZS}}$	Axial strength from the AISI & AS/NZS (4600:2018);
P_{EXP}	Axial strength from experiments;
P_{FEA}	Axial strength from the finite element analysis;
r	Radius of gyration;
r_i	Minimum radius of gyration from the AISI & AS/NZS (4600:2018);
S	Longitudinal spacing of screw;
T	Nominal thickness of the channel section;

λ_c	Non-dimensional slenderness ratio as per the AISI & AS/NZS (4600:2018);
σ	Engineering stress;
$\sigma_{\square\square\square}$	Static 0.2% proof stress;
σ_{cr}	Elastic local buckling stress of the plate;
σ_u	Static ultimate tensile strength;
ε	Engineering strain;

List of tables

Table 1 Axial strengths and failure modes of back-to-back built-up aluminium alloy channel sections

Specimen	Web	Flange	Length	Lip	Thickness	Spacing	Hole dia	Experimental results	FEA results		AISI&AS/NZS		
	h	B'	L	C'	t	S	a	P_{EXP}	P_{FEA}	P_{EXP}/P_{FEA}	$P_{AISI\&AS/NZS}$	$P_{EXP}/P_{AISI\&AS/NZS}$	Failure mode
	(mm)	(mm)	(mm)	(mm)	(mm)	(mm)	(mm)	(kN)	(kN)		(kN)		
Stub													
BU240-t1.98-L300-S50-A0	240.54	46.57	300.4	20.23	1.98	50	0	120.21	116.58	1.03	118.65	1.01	LB+DB
BU240-t1.98-L300-S50-A0.2	240.48	45.54	300.12	20.27	1.98	50	48.1	116.69	111.72	1.04	117.20	1.00	LB+DB
BU240-t1.98-L300-S50-A0.6	240.92	45.95	300.13	20.97	1.98	50	144.55	107.44	103.3	1.04	104.85	1.02	LB+DB
BU240-t1.98-L300-S200-A0	241.07	46.83	300.07	19.87	1.97	200	0	116.81	115.77	1.01	118.65	0.98	LB+DB
BU240-t1.98-L300-S200-A0.2	240.31	45.41	300.96	20.93	1.97	200	48.06	112.56	109.51	1.03	117.20	0.96	LB+DB
BU240-t1.98-L300-S200-A0.4	240.45	45.25	300.55	20.39	1.97	200	96.18	112.09	109.42	1.02	112.73	0.99	LB+DB
Mean										1.03		1.00	
COV										0.01		0.02	
Short													
BU240-t1.98-L500-S100-A0	240.83	46.76	500.03	20.07	1.98	100	0	105.71	104.66	1.01	93.80	1.13	LB+DB
BU240-t1.98-L500-S100-A0.2	240.06	45.64	500.74	20.61	1.98	100	48.01	104.23	101.62	1.03	93.02	1.12	LB+DB
BU240-t1.98-L500-S100-A0.4	240.48	45.2	500.09	20.01	1.98	100	96.19	103.81	101.21	1.03	90.69	1.14	LB+DB
BU240-t1.98-L500-S100-A0.6	240.55	45.05	500.98	20.41	1.98	100	144.33	103.72	97.82	1.07	86.80	1.19	LB+DB
BU240-t1.98-L500-S400-A0	241	46.63	499.7	20.18	1.98	400	0	106.05	106.83	0.99	93.80	1.13	LB+DB
BU240-t1.98-L500-S400-A0.2	240.72	45.89	500.66	20.05	1.98	400	48.14	105.76	104.38	1.01	93.02	1.14	LB+DB
BU240-t1.98-L500-S400-A0.4	240.11	45.23	500.81	20.65	1.98	400	96.04	105.34	103.98	1.01	90.69	1.16	LB+DB
BU240-t1.98-L500-S400-A0.6	240.54	45.69	500.11	20.82	1.98	400	144.32	103.36	99.75	1.04	86.80	1.19	LB+DB
Mean										1.02		1.15	
COV										0.02		0.03	

Note: LB=Local buckling; DB=Distortional buckling.

Table 2 Tensile coupon dimensions

Gauge length (*G*)	Width (*W*)	Thickness (*t*)	Radius of fillet (*R*)	Overall length (*L*)	Reduced parallel length (*A*)	Grip Length (*B*)	Grip width (*C*)
50 ± 0.1	12.5 ± 0.2	1.56 ± 0.05	12.6	200	57	50	20

Table 3 Material properties obtained from the tensile coupon tests

Coupon ID	Thickness, t (mm)	Ultimate stress, f_u (MPa)	Yield stress, f_y (MPa)
BU240-1	1.98	206.40	150.60
BU240-2	1.97	204.80	150.40
Mean	1.98	205.60	150.50

Table 4 Maximum amplitudes of local, distortional, and overall imperfections

Specimen	Local	Distortional	Global
	(mm)	(mm)	(mm)
BU240-t1.98-L300-S50-A0	0.41	0.88	0.89
BU240-t1.98-L300-S50-A0.2	0.55	0.69	0.94
BU240-t1.98-L300-S50-A0.6	0.28	0.79	0.82
BU240-t1.98-L300-S200-A0	0.35	0.89	1.23
BU240-t1.98-L300-S200-A0.2	0.51	1.21	0.68
BU240-t1.98-L300-S200-A0.4	0.53	0.99	1.15
BU240-t1.98-L500-S100-A0	0.60	1.12	1.27
BU240-t1.98-L500-S100-A0.2	0.46	0.75	0.81
BU240-t1.98-L500-S100-A0.4	0.89	1.02	1.02
BU240-t1.98-L500-S100-A0.6	0.68	0.98	1.11
BU240-t1.98-L500-S400-A0	0.92	0.89	1.23
BU240-t1.98-L500-S400-A0.2	0.80	1.12	1.26
BU240-t1.98-L500-S400-A0.4	0.98	0.99	1.20
BU240-t1.98-L500-S400-A0.6	1.10	0.89	1.11

Table 5 Parametric study results

Specimen	Thickness	Spacing(s)/mm For			Failure Mode(s)	P_{FEA} for plain section			P_{FEA} for section (a/h=0.2)			P_{FEA} for section (a/h=0.4)			P_{FEA} for section (a/h=0.6)			P_{FEA} for section (a/h=0.8)		
	t	2 screws	3 screws	5 screws		2 screws	3 screws	5 screws	2 screws	3 screws	5 screws	2 screws	3 screws	5 screws	2 screws	3 screws	5 screws	2 screws	3 screws	5 screws
	mm	mm	mm	mm		kN	kN	kN	kN	kN	kN	kN	kN	kN	kN	kN	kN	kN	kN	kN
BU240×45×20-L300	0.50	200	100	50	LB+DB	12.99	13.01	13.16	12.18	12.30	12.27	12.05	12.03	12.06	11.72	11.75	11.76	12.04	12.52	11.33
	1.00					43.55	44.17	44.53	42.66	43.98	44.41	43.47	42.54	42.38	40.37	41.57	40.46	37.30	36.33	43.79
	1.90					115.69	115.75	115.30	114.96	115.56	115.03	114.32	112.79	113.54	108.10	107.28	113.20	99.29	104.89	104.93
	2.10					129.91	129.95	132.02	127.64	129.84	131.71	127.61	127.30	130.57	120.38	125.97	126.67	107.67	114.11	113.23
	2.30					145.14	145.42	145.93	141.64	143.72	144.66	139.43	142.74	145.89	133.08	142.61	140.31	116.03	121.51	121.96
	2.50					160.46	160.66	160.86	157.52	160.40	160.27	151.92	159.40	158.69	146.71	159.05	156.25	124.53	131.10	130.42
	2.70					168.54	174.60	175.54	168.34	173.59	174.98	168.10	172.98	172.86	161.55	173.16	173.28	133.28	139.44	138.98
	2.90					186.33	191.84	192.84	185.99	191.18	192.08	183.17	187.30	187.05	175.12	186.52	187.36	141.75	147.81	147.30
BU240×45×20-L400	0.50	300	150	75	LB+DB	12.31	12.39	12.52	12.01	12.19	12.10	11.83	11.87	11.97	11.44	11.66	11.58	11.13	11.20	11.01
	1.00					43.09	43.16	43.61	43.12	43.03	43.19	42.61	42.56	42.70	40.88	41.30	39.98	38.17	37.78	36.54
	1.90					113.25	113.54	113.60	110.45	110.38	110.25	110.37	109.48	110.13	104.64	104.67	103.18	95.40	95.66	96.67
	2.10					126.76	127.67	127.77	124.59	124.32	123.88	121.96	122.97	122.77	116.47	118.85	117.38	103.97	105.16	105.03
	2.30					135.51	142.48	142.44	132.92	138.69	139.21	133.13	136.00	136.22	130.11	131.86	130.85	113.02	114.14	114.04
	2.50					149.60	158.47	158.52	147.39	153.98	154.62	147.20	149.82	149.63	144.52	146.70	144.77	121.45	122.88	122.81
	2.70					164.20	174.32	174.33	162.91	168.80	170.32	161.19	164.00	164.01	159.70	159.64	156.50	130.09	131.87	131.85
	2.90					181.42	185.10	191.01	178.39	181.42	185.73	180.47	178.86	178.20	170.84	173.71	170.22	138.70	141.11	139.62
BU240×45×20-L500	0.50	400	200	100	LB+DB	11.84	11.95	12.36	11.14	11.17	11.79	11.38	10.89	11.56	11.29	10.32	11.33	10.70	10.02	10.95
	1.00					43.13	43.56	43.89	42.93	43.20	43.53	42.33	42.40	43.41	38.93	39.55	40.24	34.48	34.90	34.96
	1.90					110.27	110.35	110.64	106.52	106.66	107.16	107.65	106.77	107.85	103.30	104.22	104.06	94.93	96.05	96.35
	2.10					124.59	124.68	125.04	121.61	121.27	121.60	120.76	120.70	121.46	115.22	117.23	115.64	105.40	107.05	106.62
	2.30					137.96	137.99	138.52	128.72	134.90	135.52	132.88	133.77	134.07	127.61	130.16	127.49	113.59	116.05	114.58
	2.50					152.26	152.35	153.87	142.61	148.37	150.49	143.70	145.86	147.62	141.97	145.28	142.72	122.05	123.83	122.76
	2.70					164.07	165.94	166.03	160.94	162.35	164.30	162.65	159.17	160.05	160.64	159.36	155.91	133.53	132.33	130.05
	2.90					177.70	184.42	184.74	170.62	177.20	179.81	173.87	173.80	173.96	171.45	173.03	170.63	138.89	141.29	139.21
BU240×45×20-L600	0.50	500	250	125	LB+DB	11.69	11.93	12.52	11.64	11.92	12.13	11.60	11.85	11.85	11.05	11.38	11.31	10.65	11.20	11.21
	1.00					42.60	42.88	42.94	41.24	41.82	41.74	41.96	41.06	42.60	40.27	40.41	39.60	33.56	34.59	34.92
	1.90					104.50	104.82	104.98	101.25	103.72	103.39	101.99	102.91	102.96	99.67	103.38	103.99	94.66	94.64	94.27
	2.10					117.04	117.98	118.02	115.17	117.51	116.25	115.19	117.13	117.81	112.35	117.45	117.08	105.25	104.67	104.13
	2.30					132.26	132.44	132.75	125.36	129.71	131.02	129.95	129.81	131.27	126.48	129.18	129.99	114.73	114.33	113.59
	2.50					147.10	147.26	147.90	135.51	144.90	145.87	137.18	143.21	144.85	136.35	142.86	143.72	121.93	124.40	124.05
	2.70					159.09	161.53	162.56	147.64	158.87	161.38	150.90	157.60	158.96	152.68	156.06	157.42	130.43	133.17	133.11
	2.90					179.94	179.95	180.17	164.41	174.09	177.40	167.19	172.87	173.04	168.18	169.98	171.71	139.48	141.94	142.28
BU240×45×20-L700	0.50	600	300	150	LB+DB	11.19	11.43	11.43	10.88	11.28	11.27	10.71	11.11	11.36	10.09	11.04	10.29	10.54	10.83	10.93
	1.00					41.33	41.34	42.74	41.20	41.11	42.15	40.49	40.37	42.43	40.06	40.30	40.40	34.92	34.10	34.45
	1.90					98.13	98.21	100.09	95.97	97.16	100.07	98.66	96.33	98.86	97.63	95.90	97.57	94.68	93.74	93.04

	2.10					111.49	111.64	113.12	107.94	110.34	112.58	108.94	110.14	111.48	110.14	109.55	108.24	102.73	99.05	103.05
	2.30					124.60	126.17	126.83	120.83	126.14	126.20	121.96	126.10	125.52	122.55	125.66	121.00	111.49	26.96	113.29
	2.50					140.82	141.38	141.59	139.77	139.58	140.15	140.16	139.11	139.59	136.04	139.04	139.04	122.41	121.40	123.35
	2.70					154.29	156.68	156.97	145.07	153.78	155.21	151.81	156.22	156.49	150.65	151.87	154.56	130.90	129.75	132.93
	2.90					173.32	174.55	174.93	159.50	166.79	173.03	161.00	168.29	172.84	163.61	163.26	168.76	137.85	138.65	143.77
BU240×45×20-L800	0.50	700	350	175	LB+DB	11.10	11.35	11.52	10.78	10.71	11.10	10.28	10.36	10.80	9.78	9.90	10.60	9.40	9.97	10.17
	1.00					40.83	41.35	41.90	40.73	40.90	41.89	40.25	40.60	41.77	37.62	39.00	39.02	32.94	33.53	34.29
	1.90					96.10	96.97	106.74	96.05	96.22	101.97	95.80	95.79	105.02	95.49	94.83	105.28	90.19	89.79	89.78
	2.10					107.33	108.75	120.03	104.01	107.34	119.15	103.31	106.66	118.43	103.64	105.89	116.15	101.23	100.12	99.90
	2.30					120.34	123.11	122.87	117.16	120.00	120.83	115.80	119.69	120.59	115.32	119.35	117.75	111.24	109.60	111.74
	2.50					135.14	139.51	139.62	131.46	131.75	139.38	129.60	130.93	138.45	128.71	128.22	136.72	119.85	119.68	122.61
	2.70					152.70	153.24	153.63	141.84	144.21	152.59	150.01	147.64	152.45	147.52	145.90	151.38	128.78	127.43	133.16
	2.90					169.98	170.34	170.77	154.23	157.87	170.56	161.21	156.85	169.30	160.93	153.71	162.05	136.30	136.21	141.68

Note: LB=Local buckling; DB=Distortional buckling.

Table 6 Average axial strength reduction factor (R) of investigated sections

Section type \ Screw number		2	3	5
L=300mm	a/h=0.2	0.98	0.99	0.99
	a/h=0.4	0.97	0.97	0.97
	a/h=0.6	0.93	0.96	0.95
	a/h=0.8	0.82	0.85	0.85
L=400mm	a/h=0.2	0.98	0.98	0.97
	a/h=0.4	0.98	0.96	0.96
	a/h=0.6	0.95	0.93	0.91
	a/h=0.8	0.83	0.82	0.81
L=500mm	a/h=0.2	0.96	0.97	0.98
	a/h=0.4	0.97	0.96	0.96
	a/h=0.6	0.94	0.93	0.93
	a/h=0.8	0.83	0.82	0.82
L=600mm	a/h=0.2	0.95	0.98	0.98
	a/h=0.4	0.97	0.98	0.98
	a/h=0.6	0.95	0.97	0.96
	a/h=0.8	0.85	0.86	0.85
L=700mm	a/h=0.2	0.97	0.99	0.99
	a/h=0.4	0.98	0.98	0.99
	a/h=0.6	0.97	0.97	0.96
	a/h=0.8	0.89	0.79	0.88
L=800mm	a/h=0.2	0.96	0.96	0.99
	a/h=0.4	0.97	0.96	0.98
	a/h=0.6	0.95	0.94	0.96
	a/h=0.8	0.87	0.86	0.86

Table 7 Parametric study results in terms of $P_{FEA}/P_{AISI\&AS/NZS}$

Specimen	Thickness	Spacing(s)/mm For			Failure Mode(s)	$P_{FEA}/P_{AISI\&AS/NZS}$			$P_{FEA}/P_{AISI\&AS/NZS}$			$P_{FEA}/P_{AISI\&AS/NZS}$			$P_{FEA}/P_{AISI\&AS/NZS}$			$P_{FEA}/P_{AISI\&AS/NZS}$		
						for plain section			for section (a/h=0.2)			for section (a/h=0.4)			for section (a/h=0.6)			for section (a/h=0.8)		
	t	2	3	5		2	3	5	2	3	5	2	3	5	2	3	5	2	3	5
		screws	screws	screws		screws	screws	screws	screws	screws	screws	screws	screws	screws	screws	screws	screws	screws	screws	screws
	mm	mm	mm	mm		kN	kN	kN	kN	kN	kN	kN	kN	kN	kN	kN	kN	kN	kN	kN
BU240×45×20-L300	0.5	200	100	50	LB+DB	1.30	1.29	1.30	1.24	1.24	1.23	1.29	1.28	1.28	1.38	1.37	1.37	1.67	1.73	1.56
	1					1.18	1.19	1.20	1.17	1.20	1.21	1.26	1.22	1.21	1.28	1.31	1.27	1.38	1.34	1.61
	1.9					1.06	1.05	1.05	1.07	1.07	1.06	1.10	1.08	1.09	1.12	1.10	1.17	1.17	1.22	1.22
	2.1					1.04	1.04	1.05	1.03	1.05	1.07	1.08	1.07	1.10	1.09	1.14	1.15	1.09	1.15	1.14
	2.3					1.03	1.03	1.03	1.02	1.03	1.04	1.04	1.07	1.09	1.07	1.15	1.13	1.04	1.09	1.09
	2.5					1.01	1.01	1.02	1.01	1.03	1.03	1.01	1.06	1.06	1.05	1.14	1.12	1.00	1.05	1.05
	2.7					0.96	0.99	1.00	0.97	1.00	1.01	1.01	1.04	1.04	1.05	1.12	1.12	0.97	1.01	1.01
	2.9					0.96	0.99	0.99	0.97	1.00	1.00	1.00	1.02	1.02	1.03	1.09	1.10	0.93	0.97	0.97
BU240×45×20-L400	0.5	300	150	75	LB+DB	1.25	1.24	1.25	1.24	1.24	1.23	1.27	1.25	1.26	1.31	1.32	1.30	1.42	1.41	1.39
	1					1.19	1.18	1.19	1.21	1.19	1.19	1.24	1.22	1.22	1.27	1.26	1.22	1.31	1.28	1.24
	1.9					1.22	1.22	1.22	1.20	1.20	1.20	1.23	1.22	1.23	1.23	1.23	1.21	1.20	1.21	1.22
	2.1					1.20	1.21	1.21	1.19	1.19	1.18	1.20	1.21	1.21	1.21	1.23	1.22	1.16	1.17	1.17
	2.3					1.14	1.20	1.20	1.13	1.18	1.18	1.17	1.19	1.19	1.20	1.22	1.21	1.13	1.14	1.14
	2.5					1.13	1.20	1.20	1.12	1.18	1.18	1.16	1.18	1.18	1.20	1.22	1.20	1.09	1.10	1.10
	2.7					1.12	1.19	1.19	1.12	1.16	1.17	1.15	1.17	1.17	1.20	1.20	1.17	1.05	1.07	1.07
	2.9					1.13	1.15	1.18	1.12	1.14	1.16	1.17	1.16	1.15	1.16	1.18	1.16	1.02	1.04	1.03
BU240×45×20-L500	0.5	400	200	100	LB+DB	1.24	1.22	1.26	1.18	1.15	1.21	1.24	1.16	1.22	1.30	1.16	1.26	1.34	1.22	1.33
	1					1.23	1.21	1.21	1.24	1.21	1.21	1.26	1.22	1.24	1.21	1.20	1.21	1.16	1.15	1.14
	1.9					1.27	1.27	1.27	1.24	1.24	1.24	1.28	1.27	1.28	1.29	1.30	1.29	1.26	1.27	1.28
	2.1					1.24	1.24	1.25	1.22	1.22	1.22	1.25	1.25	1.25	1.24	1.27	1.25	1.22	1.23	1.23
	2.3					1.21	1.21	1.21	1.14	1.19	1.20	1.20	1.21	1.21	1.21	1.23	1.21	1.15	1.18	1.16
	2.5					1.18	1.18	1.19	1.11	1.16	1.18	1.15	1.17	1.18	1.19	1.22	1.20	1.10	1.11	1.10
	2.7					1.14	1.15	1.15	1.13	1.14	1.15	1.17	1.14	1.15	1.21	1.20	1.17	1.07	1.06	1.04
	2.9					1.11	1.15	1.16	1.08	1.12	1.14	1.13	1.13	1.13	1.16	1.17	1.16	1.01	1.02	1.01
BU240×45×20-L600	0.5	500	250	125	LB+DB	1.27	1.25	1.29	1.28	1.25	1.26	1.30	1.28	1.27	1.29	1.28	1.26	1.33	1.32	1.31
	1					1.27	1.27	1.27	1.24	1.24	1.24	1.29	1.24	1.29	1.29	1.27	1.24	1.14	1.11	1.12
	1.9					1.22	1.22	1.22	1.19	1.22	1.21	1.22	1.23	1.23	1.24	1.29	1.30	1.25	1.22	1.22
	2.1					1.17	1.18	1.18	1.16	1.19	1.17	1.19	1.21	1.22	1.20	1.26	1.25	1.19	1.16	1.16
	2.3					1.16	1.16	1.16	1.11	1.14	1.16	1.17	1.17	1.18	1.18	1.21	1.22	1.12	1.11	1.10
	2.5					1.14	1.14	1.15	1.06	1.13	1.14	1.09	1.14	1.16	1.13	1.18	1.19	1.05	1.07	1.07
	2.7					1.10	1.12	1.13	1.03	1.11	1.13	1.08	1.12	1.13	1.13	1.16	1.17	1.00	1.02	1.02
	2.9					1.13	1.13	1.13	1.04	1.10	1.12	1.08	1.11	1.11	1.12	1.14	1.15	0.97	0.99	0.99

BU240×45×20-L700	0.5	600	300	150	LB+DB	1.27	1.22	1.21	1.24	1.22	1.20	1.25	1.22	1.23	1.22	1.26	1.16	1.31	1.27	1.27
	1					1.29	1.28	1.32	1.29	1.28	1.31	1.30	1.28	1.35	1.33	1.32	1.32	1.19	1.14	1.15
	1.9					1.14	1.14	1.16	1.12	1.14	1.17	1.18	1.15	1.18	1.20	1.18	1.20	1.20	1.19	1.18
	2.1					1.12	1.12	1.13	1.09	1.11	1.13	1.12	1.13	1.14	1.17	1.16	1.15	1.12	1.08	1.13
	2.3					1.09	1.10	1.11	1.06	1.11	1.11	1.09	1.13	1.13	1.14	1.16	1.12	1.06	0.26	1.08
	2.5					1.09	1.10	1.10	1.09	1.09	1.09	1.11	1.11	1.11	1.12	1.14	1.14	1.03	1.03	1.04
	2.7					1.07	1.09	1.09	1.01	1.07	1.08	1.08	1.11	1.11	1.10	1.11	1.13	0.99	0.98	1.00
	2.9					1.09	1.09	1.10	1.00	1.05	1.09	1.03	1.08	1.11	1.08	1.08	1.12	0.94	0.95	0.98
BU240×45×20-L800	0.5	700	350	175	LB+DB	1.33	1.25	1.25	1.30	1.19	1.21	1.26	1.17	1.20	1.23	1.15	1.21	1.21	1.19	1.19
	1					1.35	1.29	1.31	1.35	1.28	1.32	1.36	1.30	1.33	1.31	1.28	1.28	1.16	1.12	1.15
	1.9					1.14	1.13	1.24	1.14	1.13	1.19	1.16	1.14	1.25	1.18	1.16	1.29	1.13	1.12	1.12
	2.1					1.11	1.09	1.20	1.08	1.08	1.20	1.09	1.09	1.21	1.11	1.12	1.22	1.10	1.08	1.08
	2.3					1.10	1.08	1.08	1.07	1.06	1.06	1.07	1.07	1.08	1.09	1.10	1.08	1.06	1.03	1.05
	2.5					1.10	1.08	1.08	1.07	1.03	1.09	1.07	1.04	1.10	1.09	1.04	1.11	1.02	1.00	1.02
	2.7					1.12	1.06	1.07	1.04	1.01	1.06	1.11	1.05	1.08	1.12	1.06	1.10	0.99	0.95	0.99
	2.9					1.12	1.07	1.07	1.02	0.99	1.07	1.08	1.00	1.08	1.10	1.01	1.06	0.94	0.92	0.95

Table 8 Comparisons of axial strength reduction factors obtained from the experiments and proposed design equations

Specimen	*a/h*	Experimental results	R_{EXP}	R_{prop}	R_{EXP}/R_{prop}
		P_{EXP}			
		(kN)			
Stub					
BU240-t1.98-L300-S50-A0.2	0.2	116.69	0.97	0.98	0.99
BU240-t1.98-L300-S50-A0.6	0.6	107.44	0.89	0.93	0.96
BU240-t1.98-L300-S200-A0.2	0.2	112.56	0.96	0.98	0.99
BU240-t1.98-L300-S200-A0.4	0.4	112.09	0.96	0.97	0.99
Mean					0.98
COV					0.01
Stub					
BU240-t1.98-L500-S100-A0.2	0.2	104.23	0.99	0.97	1.01
BU240-t1.98-L500-S100-A0.4	0.4	103.81	0.98	0.97	1.01
BU240-t1.98-L500-S100-A0.6	0.6	103.72	0.98	0.96	1.03
BU240-t1.98-L500-S400-A0.2	0.2	105.76	0.99	0.97	1.02
BU240-t1.98-L500-S400-A0.4	0.4	105.34	0.99	0.97	1.02
BU240-t1.98-L500-S400-A0.6	0.6	103.36	0.97	0.96	1.02
Mean					1.02
COV					0.01

Table 9 Results of the reliability analysis for proposed strength reduction factor equations of aluminium BTB channels with web holes

Column type	Stub column	Short column
Ratio of equations	R_{FEA} / R_{prop}	R_{FEA} / R_{prop}
Data number	256	320
Mean, P_{m}	1.00	1.00
Coefficient of variation, COV	0.04	0.06
Reliability index, β [12]	2.70	2.70
Resistance factor, φ [12]	0.85	0.85

List of figures

(a) BU240-t1.98-L300-S50

(b) BU240-t1.98-L300-S200

(c) BU240-t1.98-L500-S100

(d) BU240-t1.98-L500-S400

Fig.14 Effect of hole size on axial strength of aluminium BTB channels

(a) BU240-t1.98-L300-S50

(b) BU240-t1.98-L300-S200

(c) BU240-t1.98-L500-S100

(d) BU240-t1.98-L500-S400

Fig.15 Details of the FE model

(a) Mesh type and boundary condition applied in FE model for BU240-t1.98-L300-S200-A0.4

(b) Initial imperfection contours

Fig.16 Deformed shapes at failure from experiments and FEA

(a) BU240-t1.98-L300-S50-A0.2

(b) BU240-t1.98-L300-S50-A0.6

(c) BU240-t1.98-L300-S200-A0.2

(d) BU240-t1.98-L300-S200-A0.4

(e) BU240-t1.98-L500-S100-A0.2

(f) BU240-t1.98-L500-S100-A0.4

(g) BU240-t1.98-L500-S100-A0.6

(h) BU240-t1.98-L500-S400-A0.2

(i) BU240-t1.98-L500-S400-A0.4

(j) BU240-t1.98-L500-S400-A0.4

Fig.17 Load versus axial-shortening relationship for columns

(a) BU240-t1.98-L300-S50-A0.2

(b) BU240-t1.98-L300-S50-A0.6

(c) BU240-t1.98-L300-S200-A0.2

(d) BU240-t1.98-L500-S100-A0.2

(e) BU240-t1.98-L500-S100-A0.4

(f) BU240-t1.98-L500-S100-A0.6

(g) BU240-t1.98-L500-S400-A0.2

(h) BU240-t1.98-L500-S400-A0.6

Fig.18 Parametric effects on axial strength of investigated sections

(a) Axial strength of sections against the ratio of *a/h*

(b) Axial strength of sections against screw number

(c) Axial strength of sections against section thickness

(d) Axial strength of sections against column length

(e) Axial strength of sections against modified slenderness

Fig.19 Parametric effects on axial strength reduction factor of investigated sections

(a) Strength reduction factor of sections against the ratio of *a/h*

(b) Strength reduction factor of sections against screw number

(c) Strength reduction factor of sections against section thickness

(d) Strength reduction factor of sections against column length

(e) Strength reduction factor of sections against modified slenderness

Fig.20 Comparison of axial strengths obtained from the FEA and the current design standards (AISI & AS/NZS)

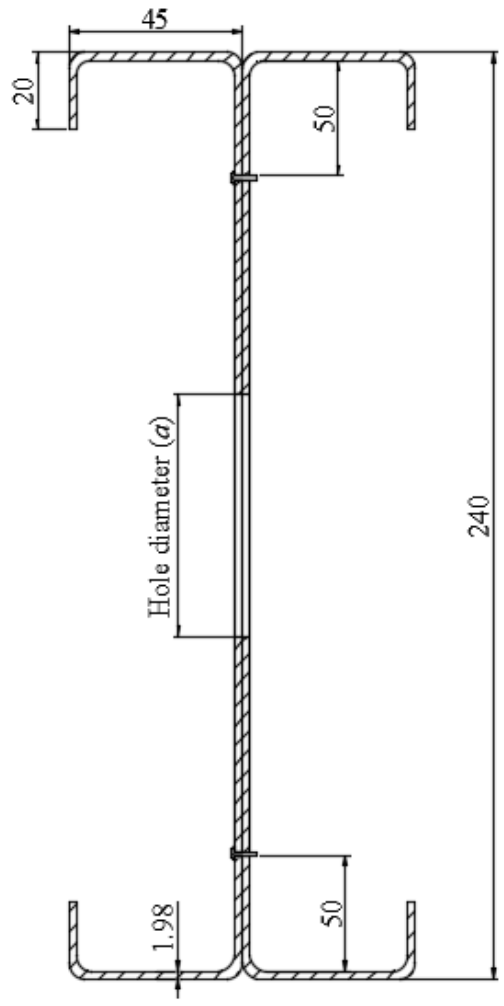

(All dimensions are in mm)

Fig.1 Cross-sectional details of the investigated aluminium alloy built-up channels with web holes

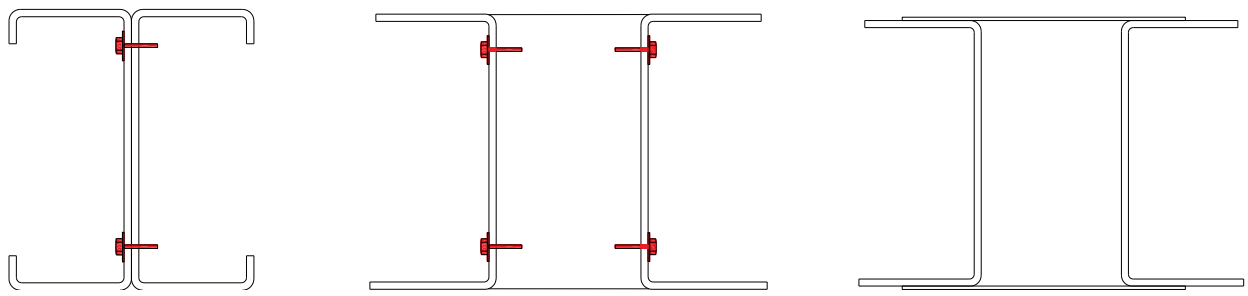

(a) Roy *et al*. [17-19] (b) Roy *et al*. [20-21] (c) Dabaon *et al*. [24-25] and Anbarasu *et al*. [26−27]

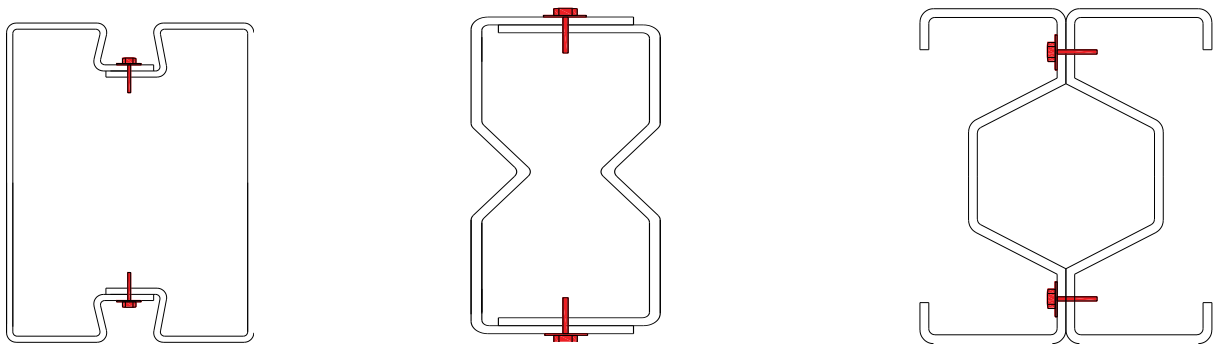

(d) Roy *et al*. [28] (e) Zhang and Young [29] (f) Zhang and Young [30-31]

Fig.2 Cross-section of various built-up columns from the literature

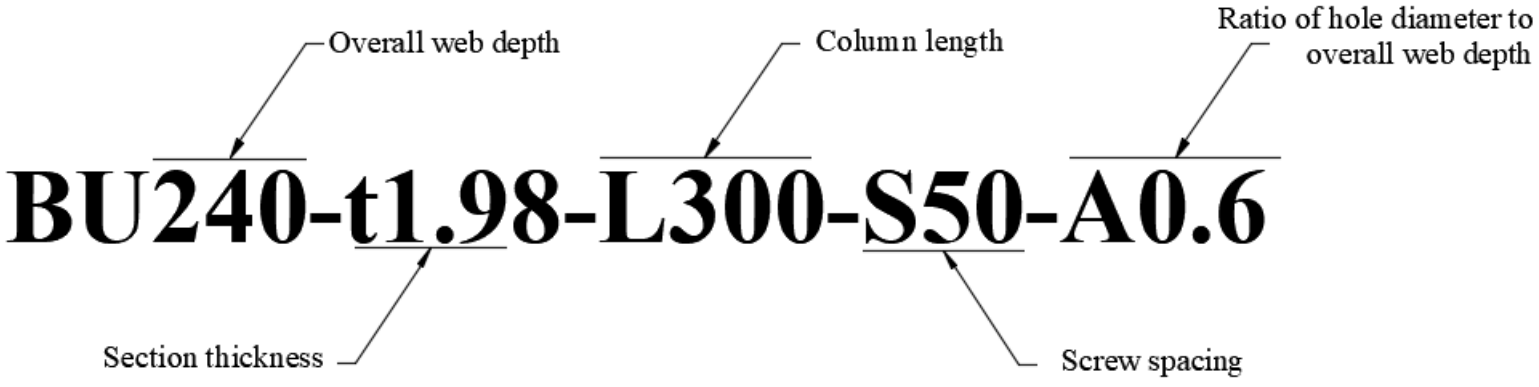

Fig.3 Specimen labelling

Fig.4 Setup of the tensile coupon tests

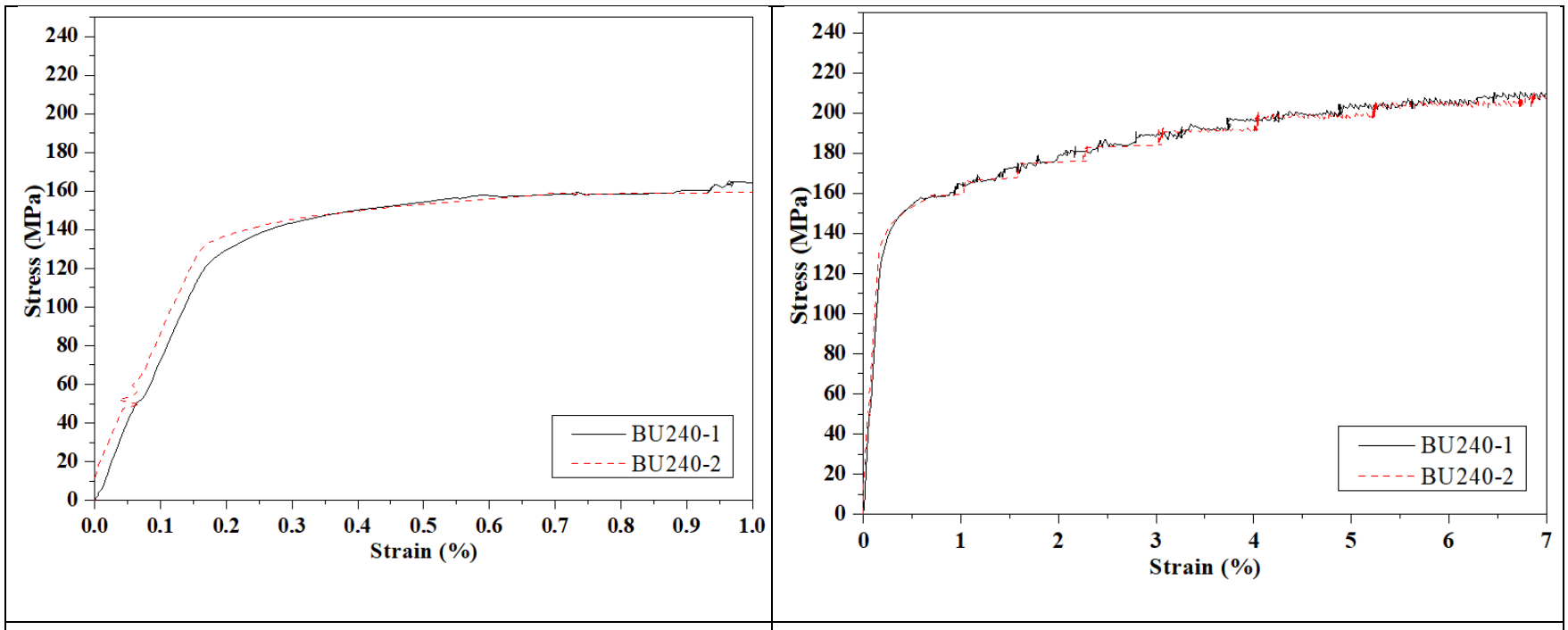

(a) Initial stress–strain curve | (b) Full stress–strain curve

Fig.5 Stress-strain curves [14]

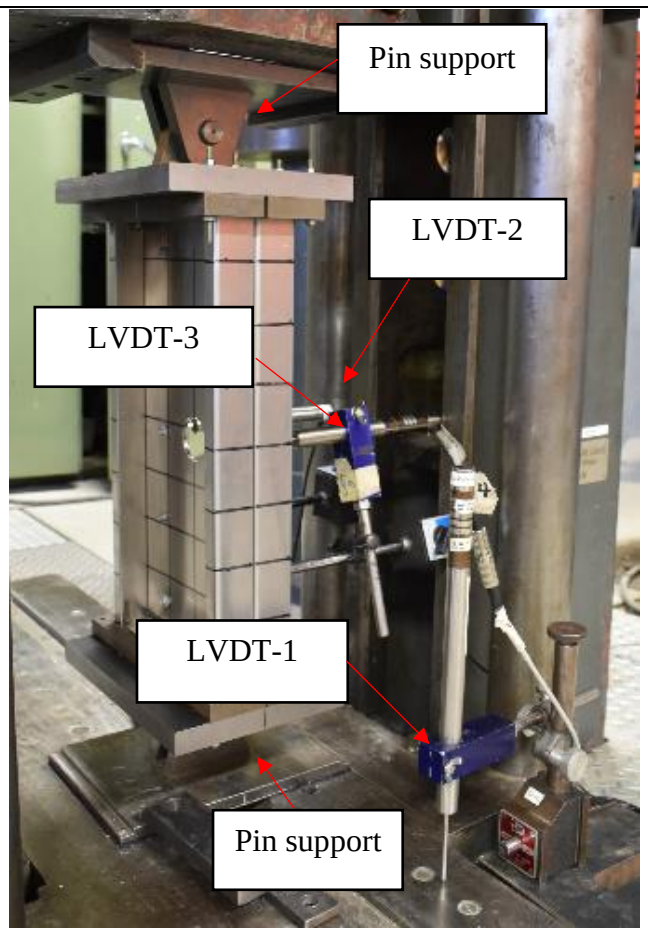

(a) Photograph

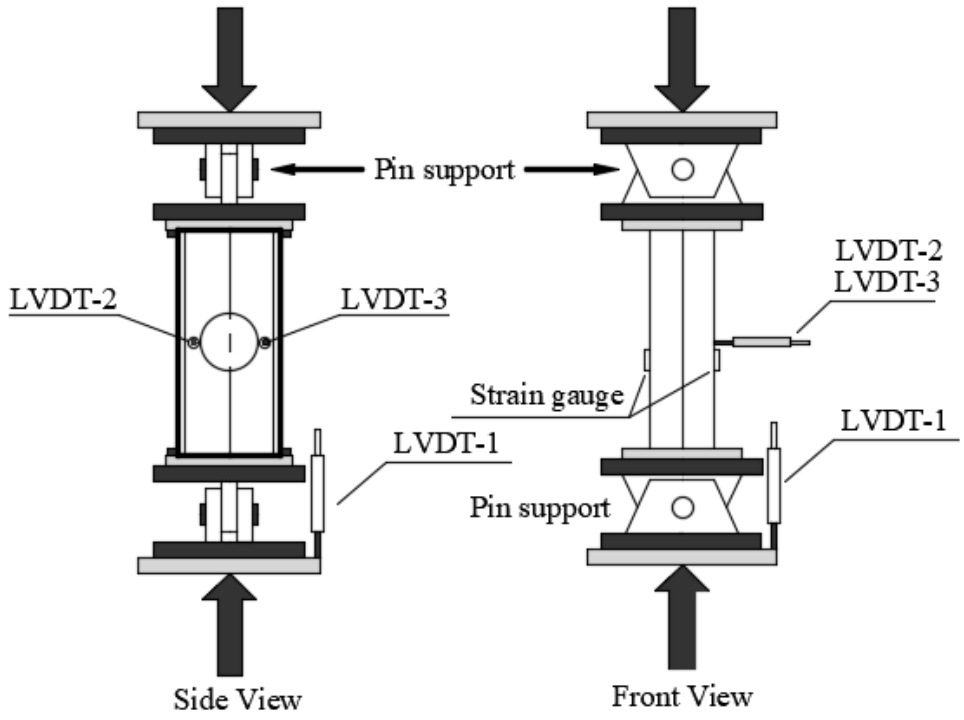

(b) Schematic drawing

Fig.6 Photograph and schematic drawings of the test set-up

(a) Bottom support

(b) Top support

Fig.7 End plates used in compression tests

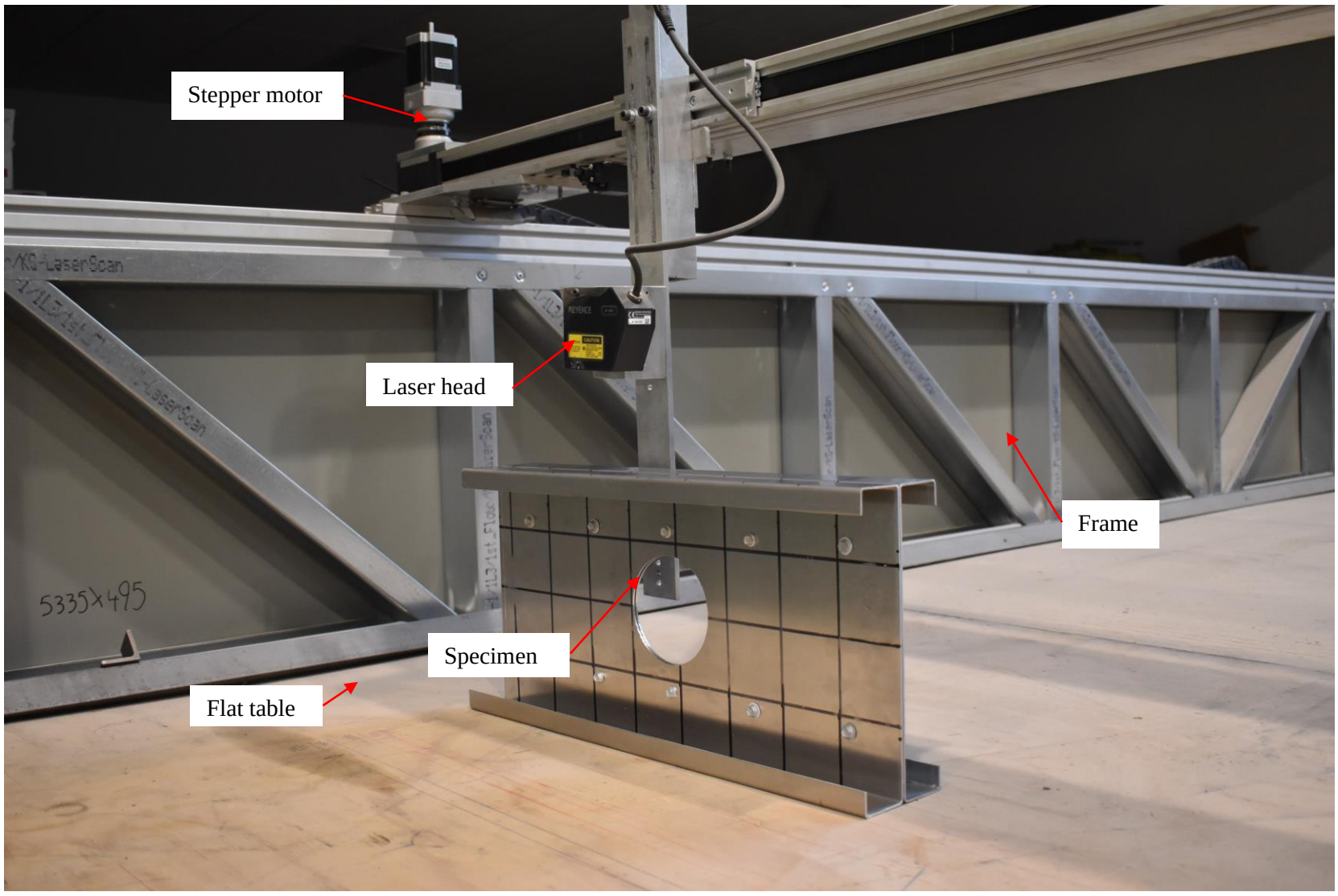

Fig.8 Imperfection measurements setup

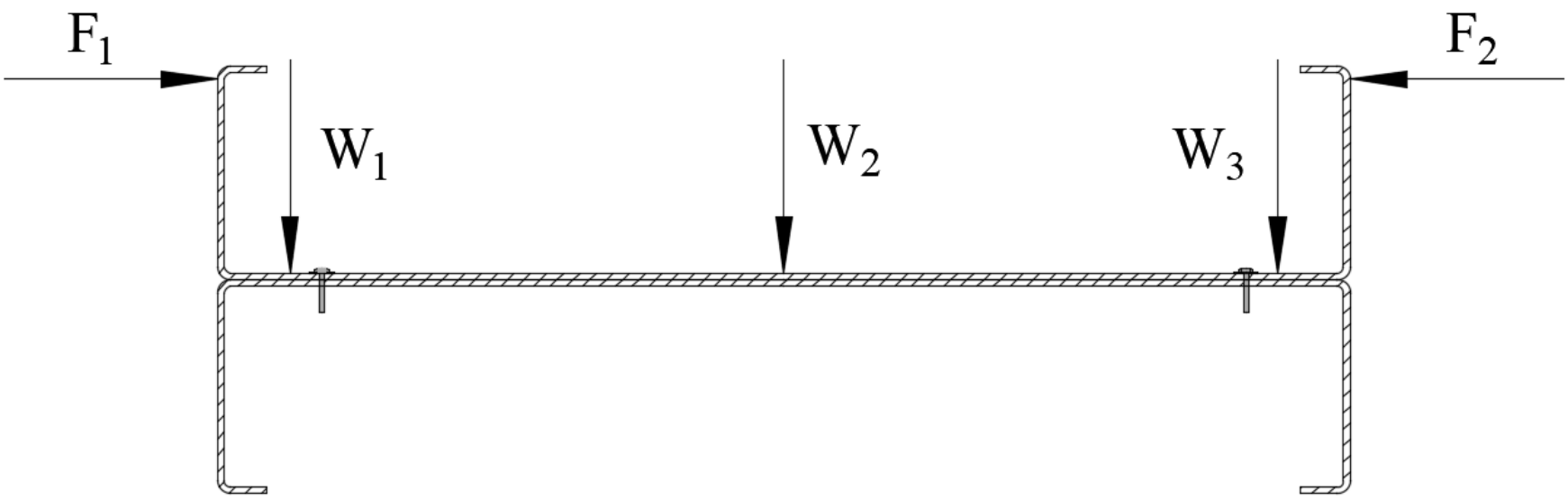

Fig.9 Locations of the initial geometric imperfection measurements

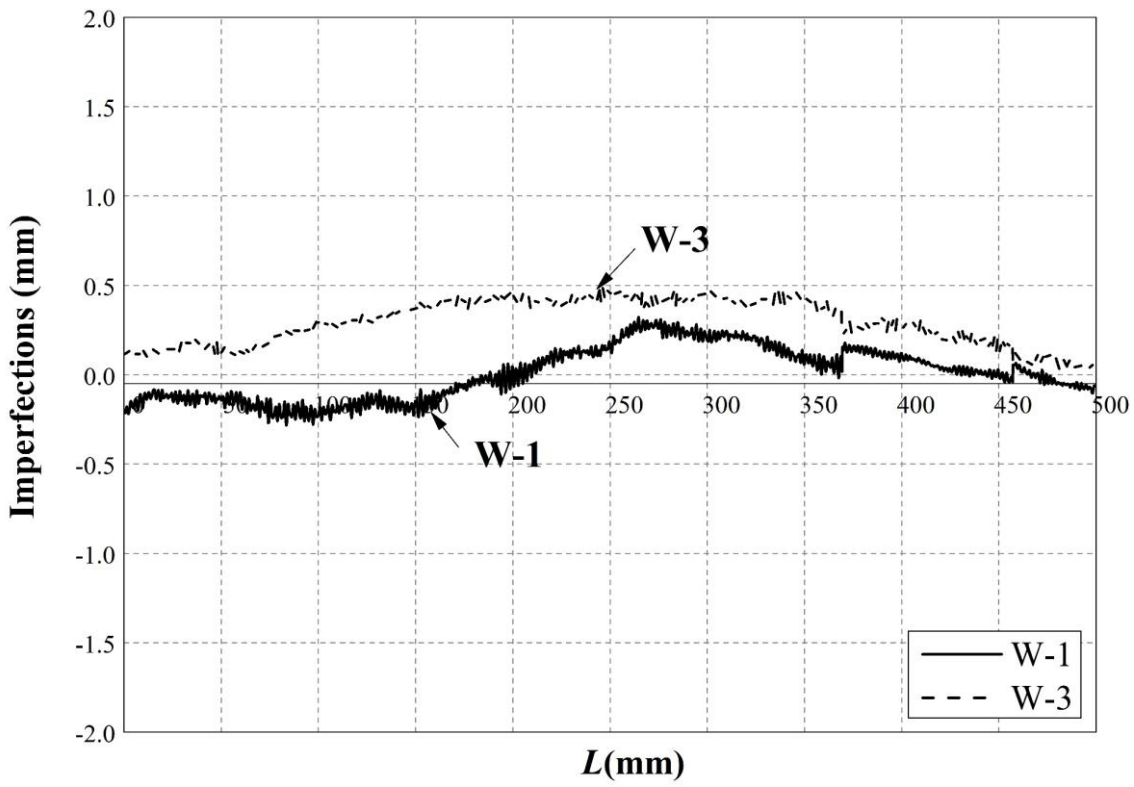

(a) Imperfection of W-1 and W-3

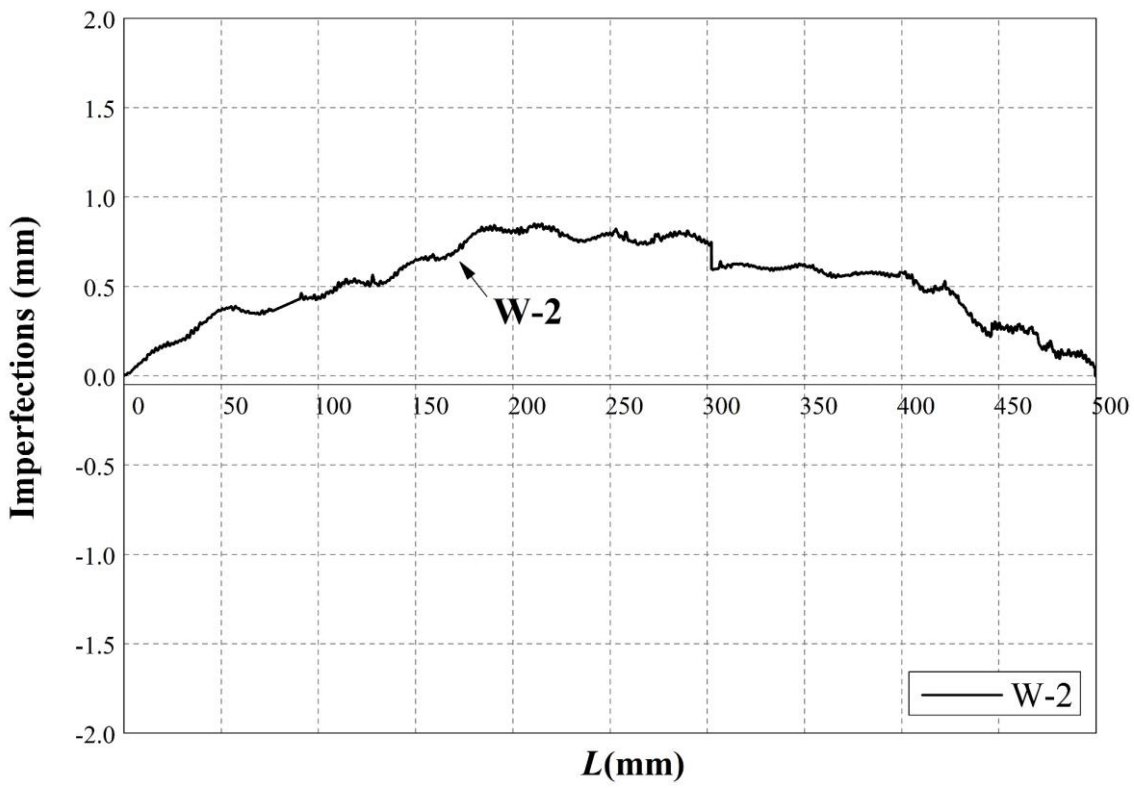

(b) Imperfection of W-2

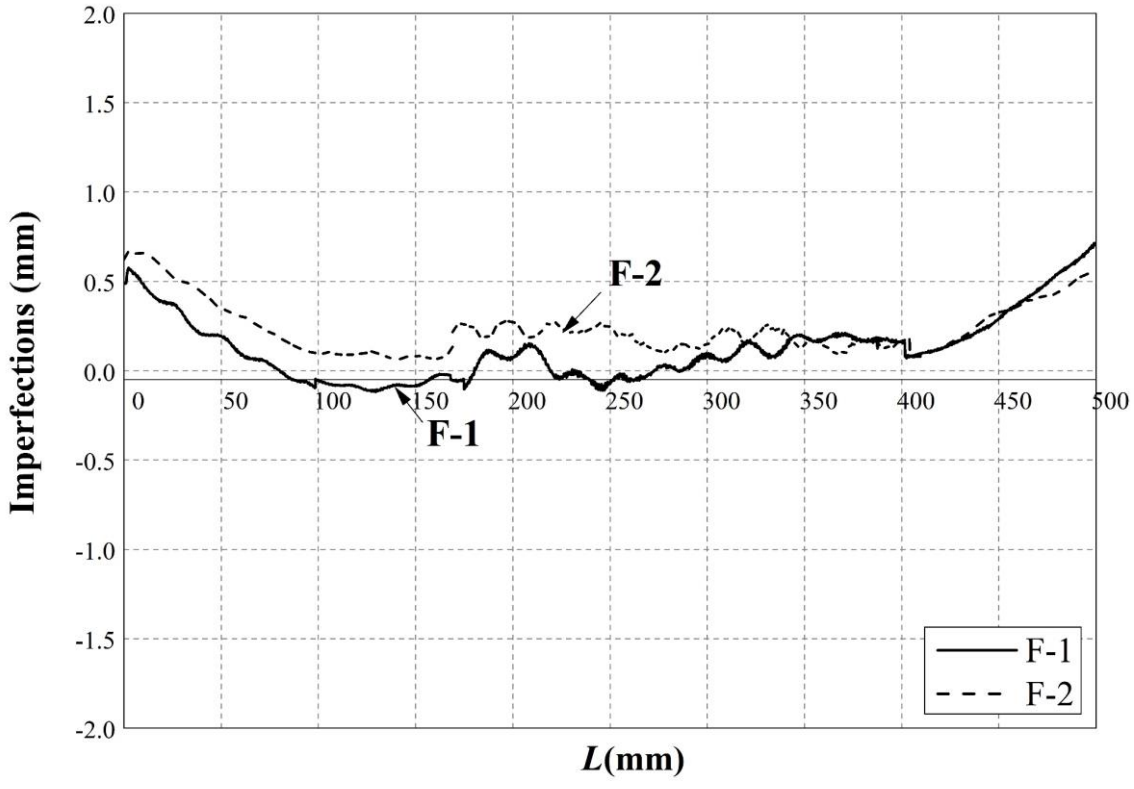

(c) Imperfection of F-1 and F-2

Fig.10 Typical imperfection profile (BU240-t1.98-L500-S100-A0.2)

			
(a) BU240-t1.98-L300-S50-A0.2	(b) BU240-t1.98-L300-S200-A0.2	(c) BU240-t1.98-L500-S100-A0.2	(d) BU240-t1.98-L500-S400-A0.2

Fig.11 Test pictures of the 300- and 500mm-long sections

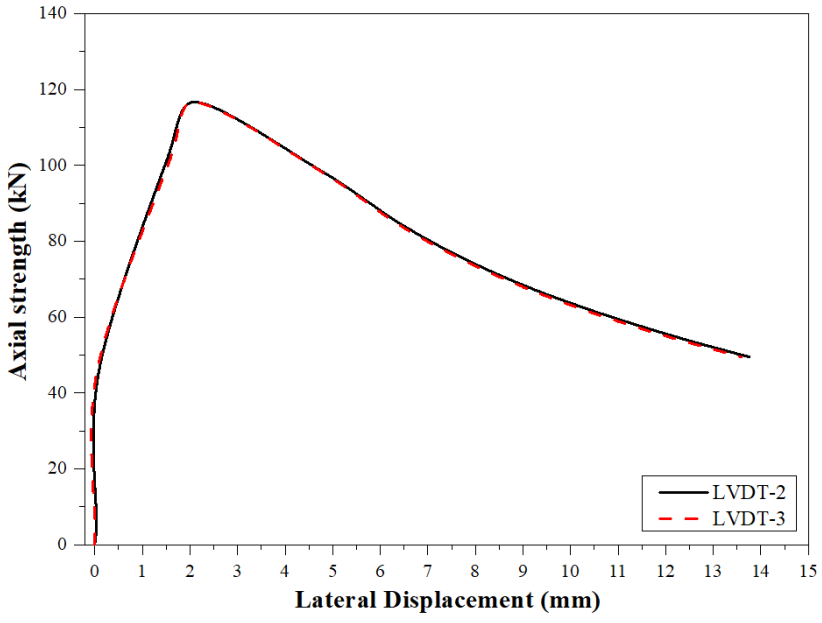

(a) BU240-t1.98-L300-S50-A0.2

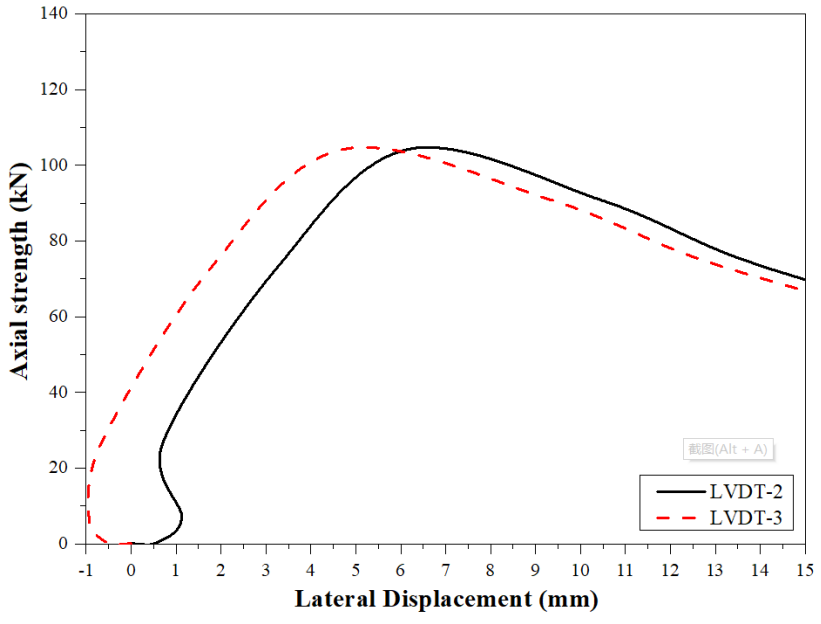

(b) BU240-t1.98-L500-S100-A0.2

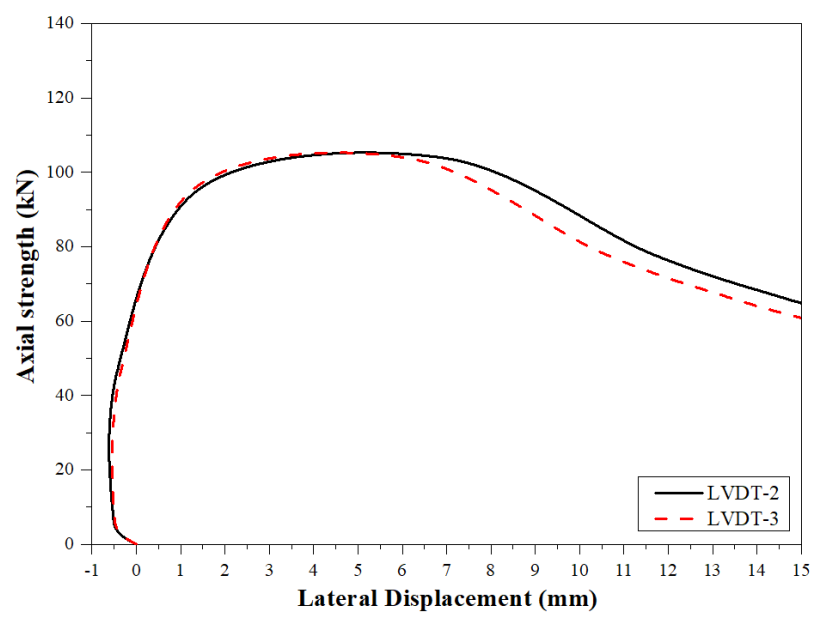

(c) BU240-t1.98-L300-S50-A0.2

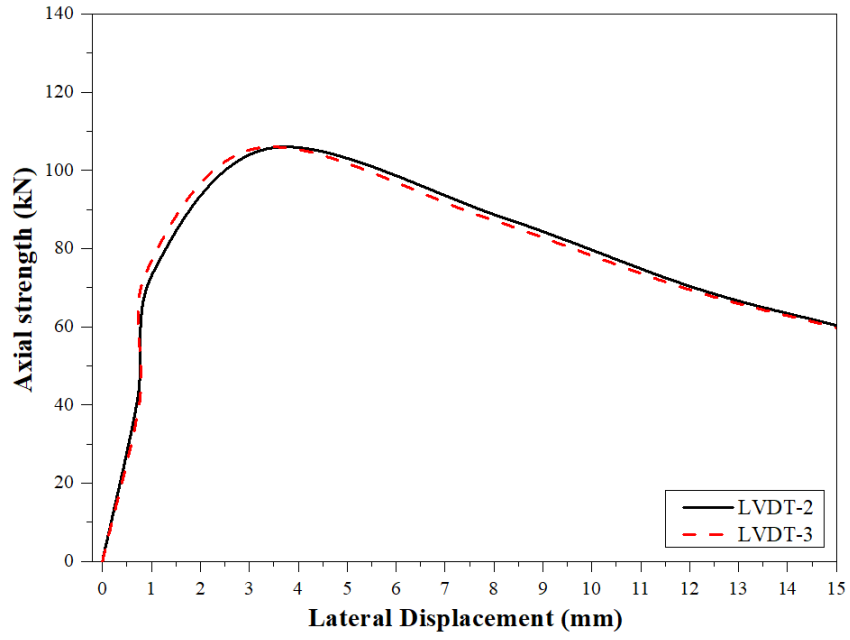

(d) BU240-t1.98-L500-S400-A0.2

Fig.12 Load versus lateral deflection curves at mid-height

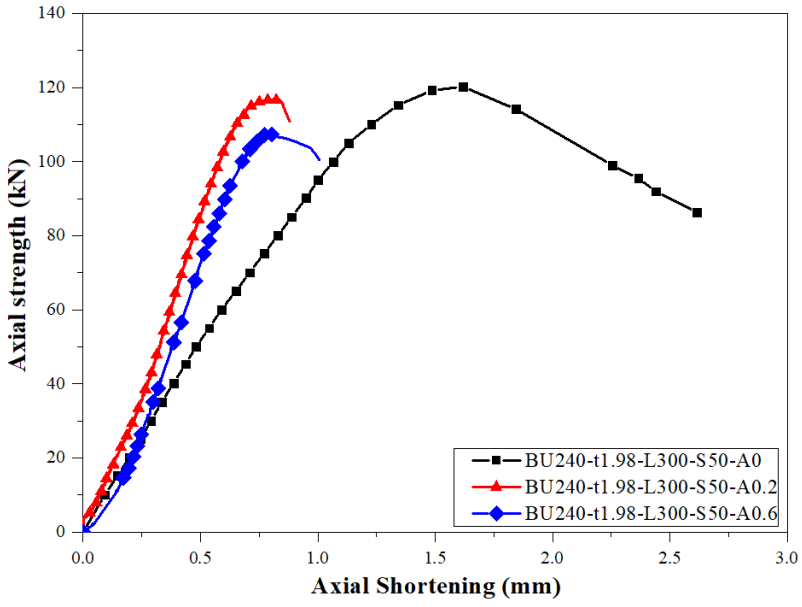

(a) BU240-t1.98-L300-S50

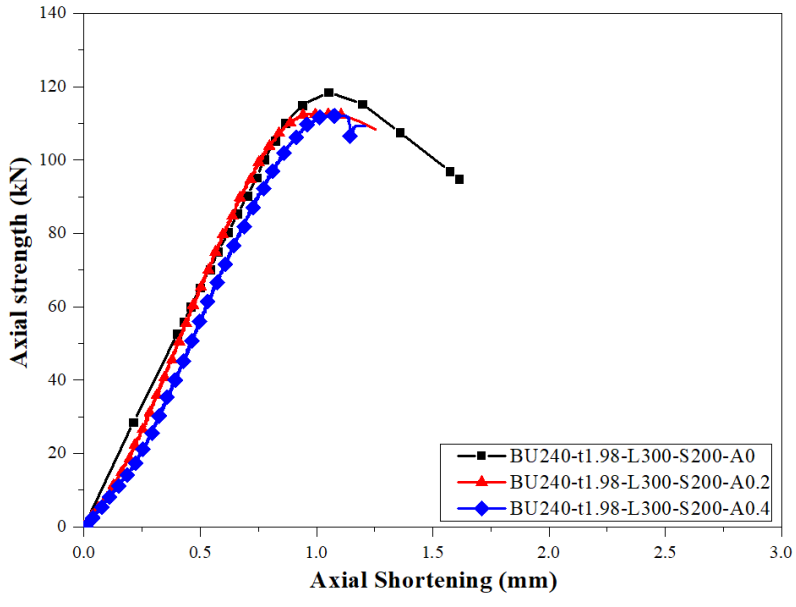

(b) BU240-t1.98-L300-S200

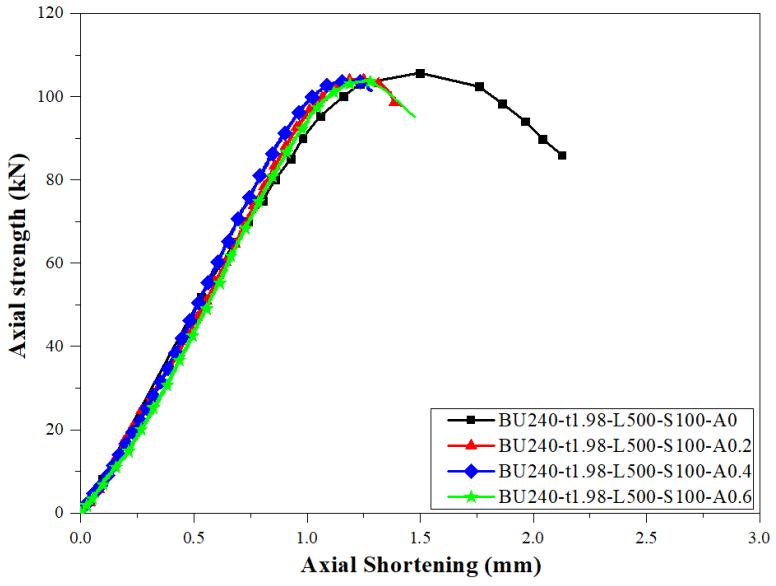

(c) BU240-t1.98-L500-S100

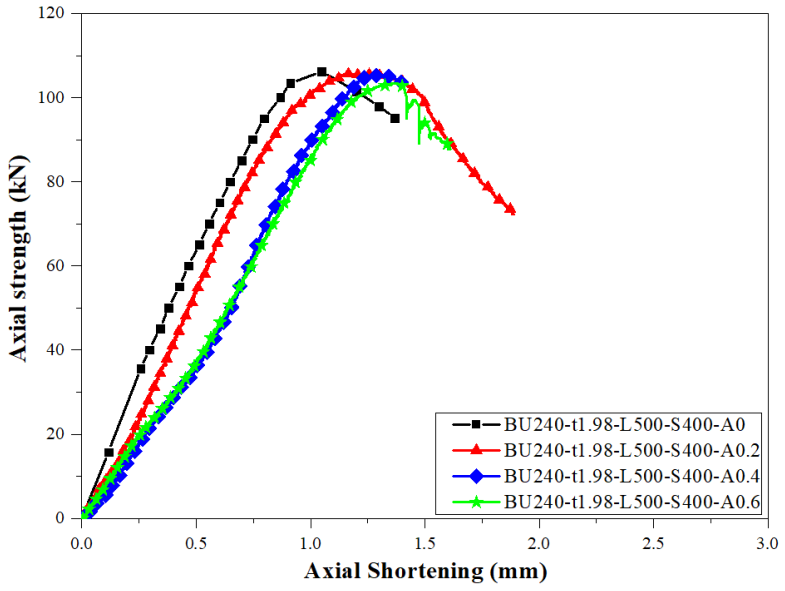

(d) BU240-t1.98-L500-S400

Fig.13 Axial load versus axial shortening curves

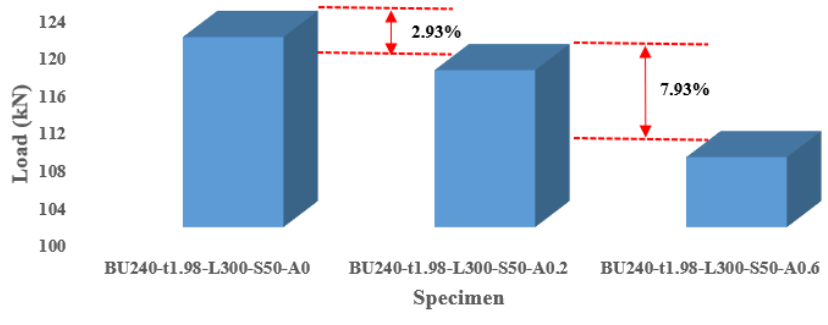

(a) BU240-t1.98-L300-S50

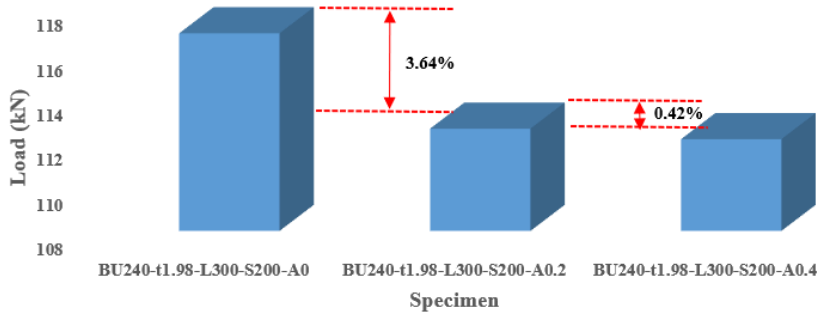

(b) BU240-t1.98-L300-S200

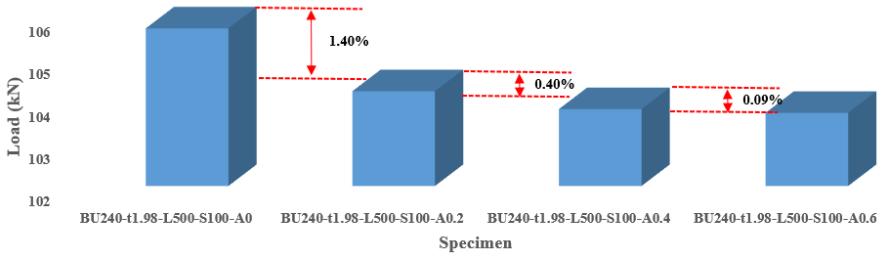

(c) BU240-t1.98-L500-S100

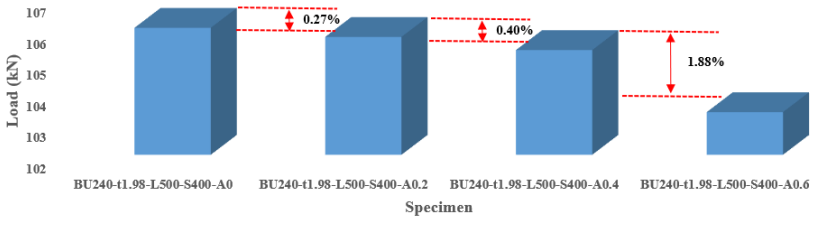

(d) BU240-t1.98-L500-S400

Fig.14 Effect of hole size on axial strength of aluminium BTB channels

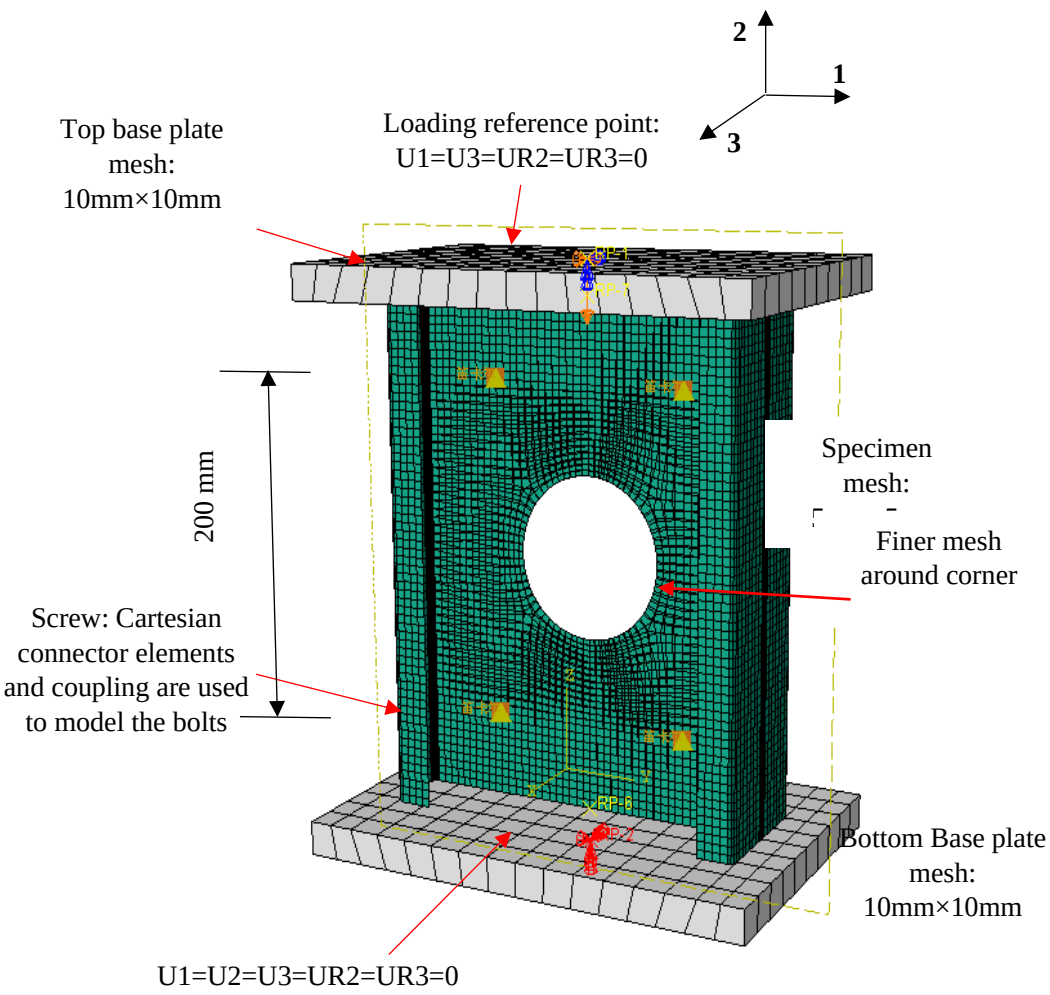

(a) Mesh type and boundary condition applied in FE model for BU240-t1.98-L300-S200-A0.4

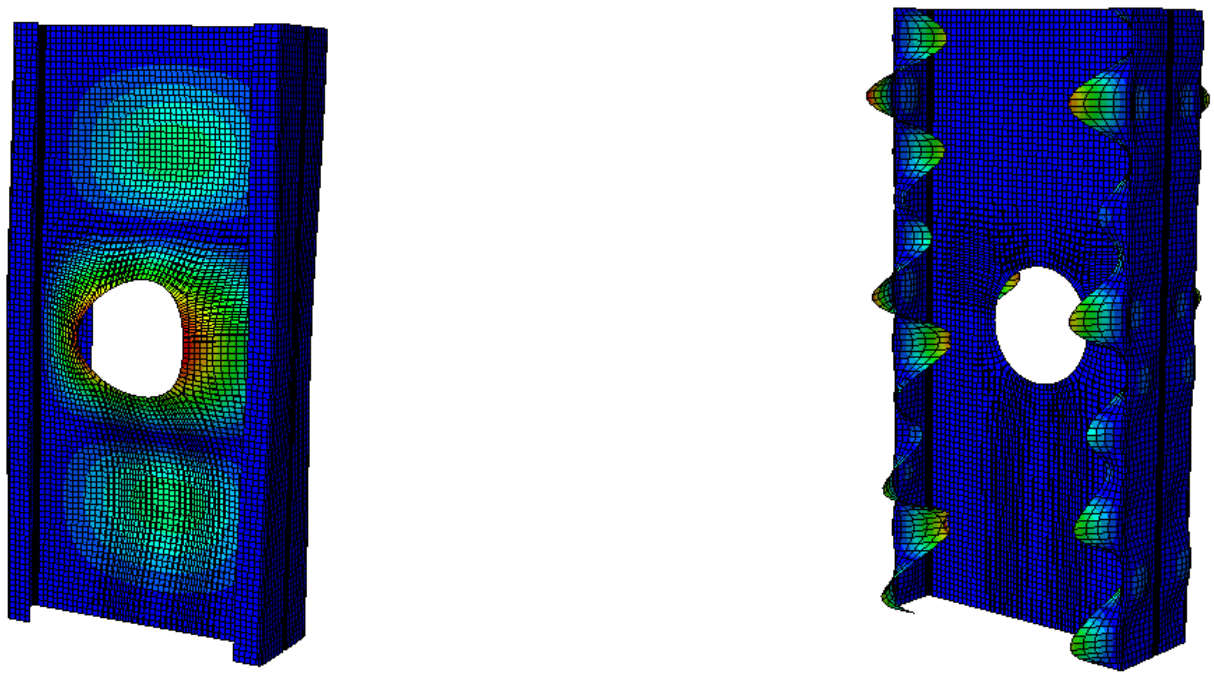

(i) Local buckling (ii) Distortional buckling

(b) Initial imperfection contours from eigenvalue buckling analysis

Fig.15 Details of the FE model

	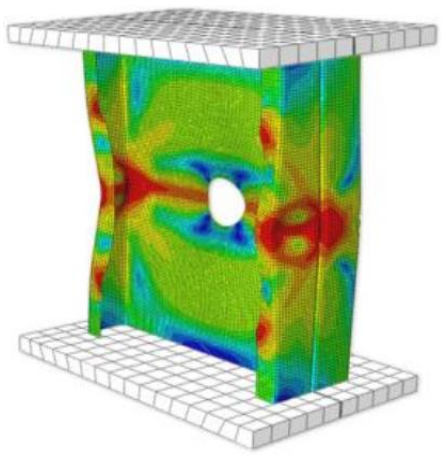	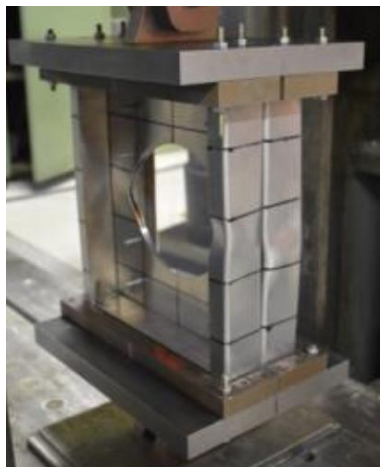	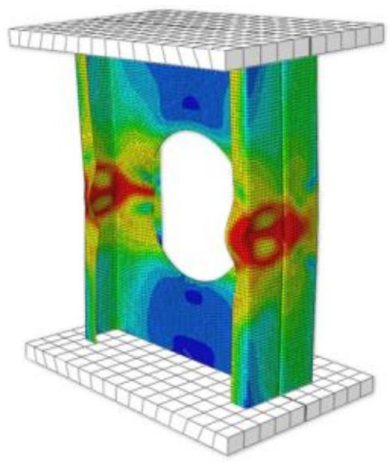
(i) Test	(ii) FEA	(i) Test	(ii) FEA
(a) BU240-t1.98-L300-S50-A0.2		(b) BU240-t1.98-L300-S50-A0.6	
	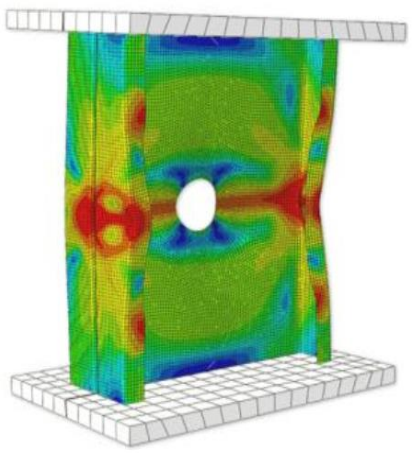	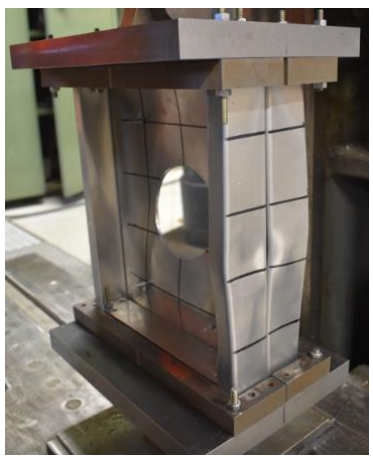	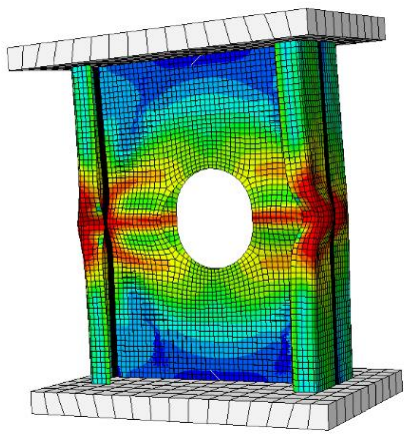
(i) Test	(ii) FEA	(i) Test	(ii) FEA
(c) BU240-t1.98-L300-S200-A0.2		(d) BU240-t1.98-L300-S200-A0.4	
	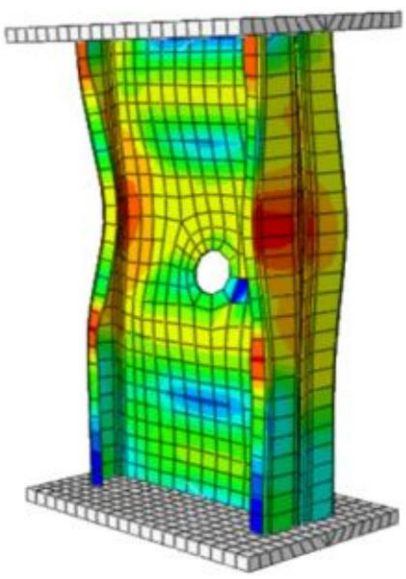		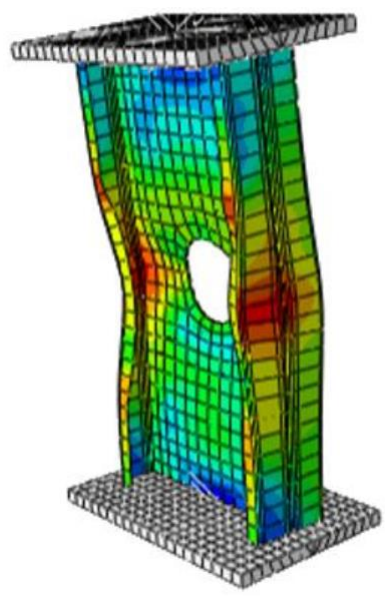
(i) Test	(ii) FEA	(i) Test	(ii) FEA
(e) BU240-t1.98-L500-S100-A0.2		(f) BU240-t1.98-L500-S100-A0.4	
	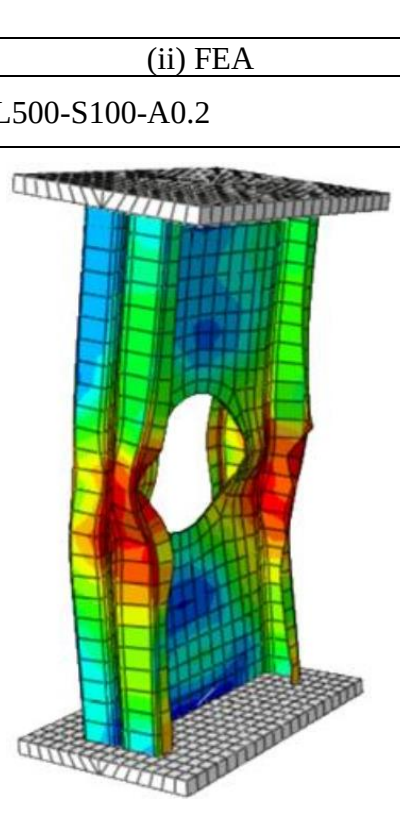		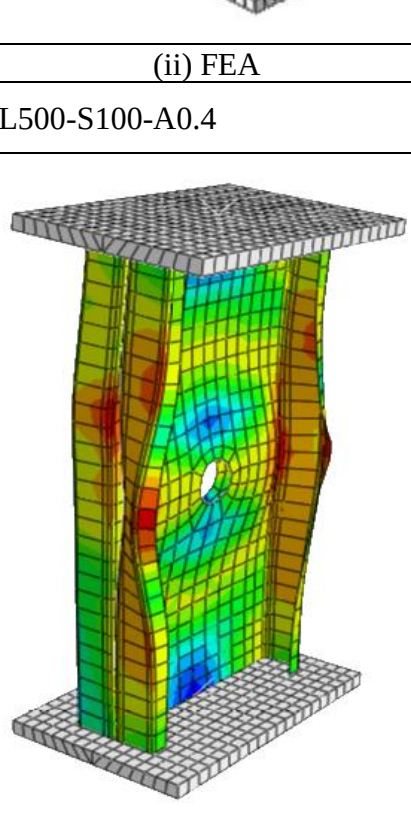
(i) Test	(ii) FEA	(i) Test	(ii) FEA
(g) BU240-t1.98-L500-S100-A0.6		(h) BU240-t1.98-L500-S400-A0.2	

	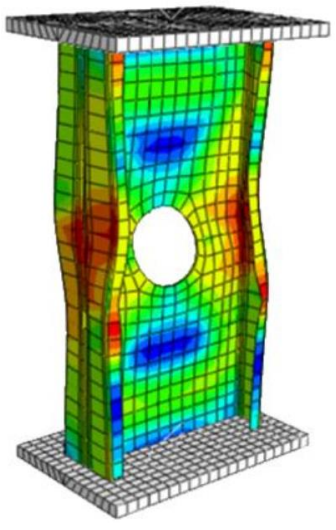	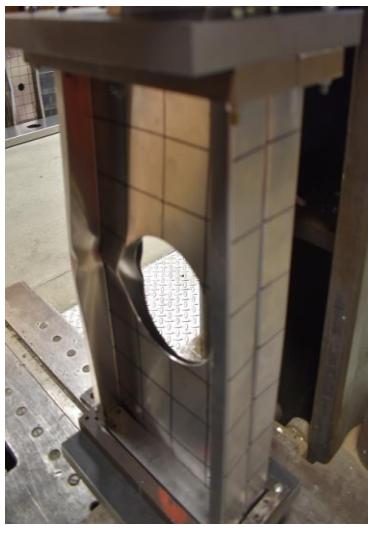	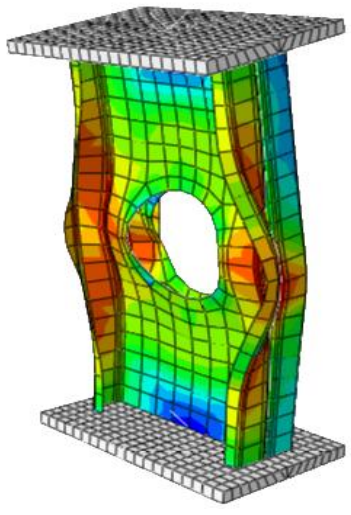
(i) Test	(ii) FEA	(i) Test	(ii) FEA
(i) BU240-t1.98-L500-S400-A0.4		(j) BU240-t1.98-L500-S400-A0.4	

Fig.16 Deformed shapes at failure from experiments and FEA

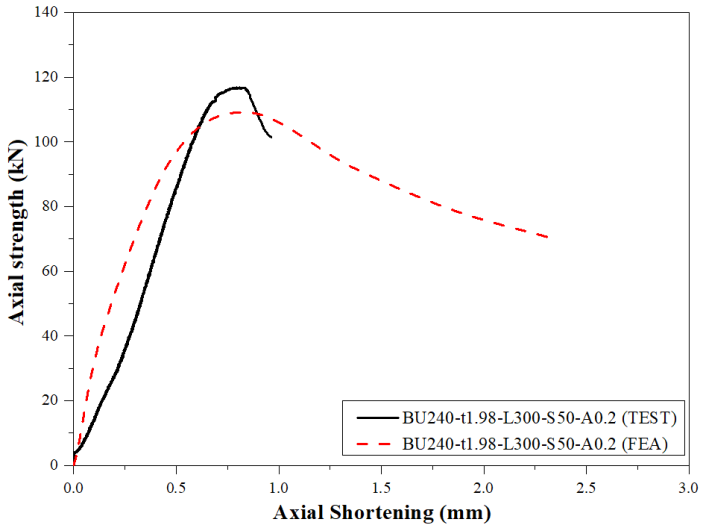

(a) BU240-t1.98-L300-S50-A0.2

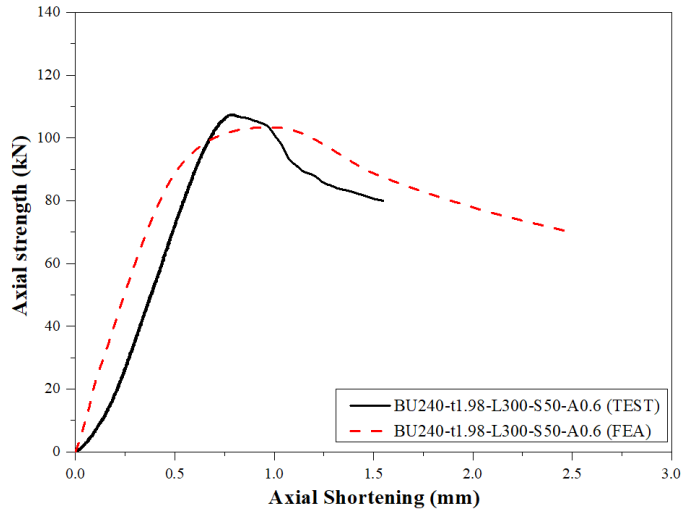

(b) BU240-t1.98-L300-S50-A0.6

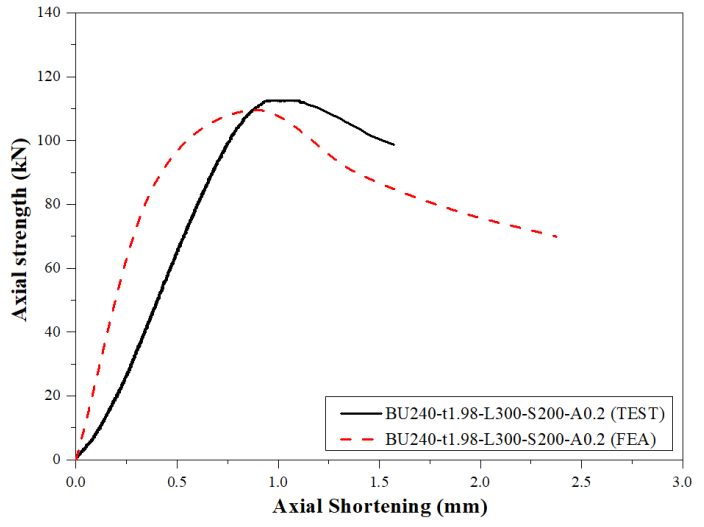

(c) BU240-t1.98-L300-S200-A0.2

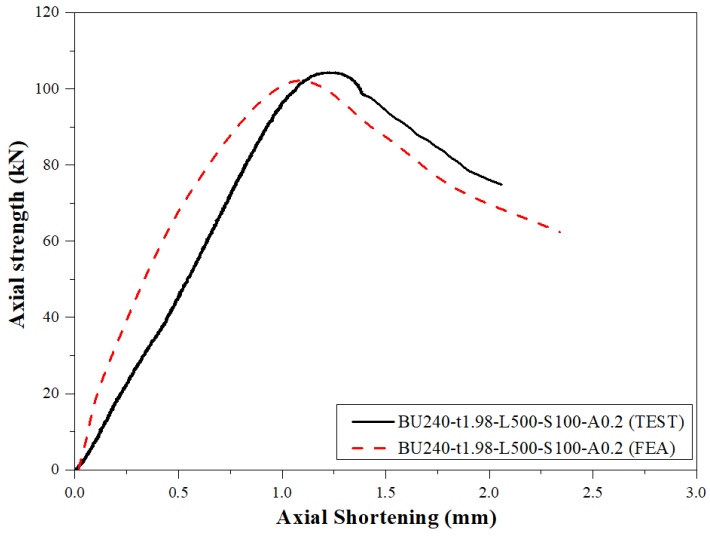

(d) BU240-t1.98-L500-S100-A0.2

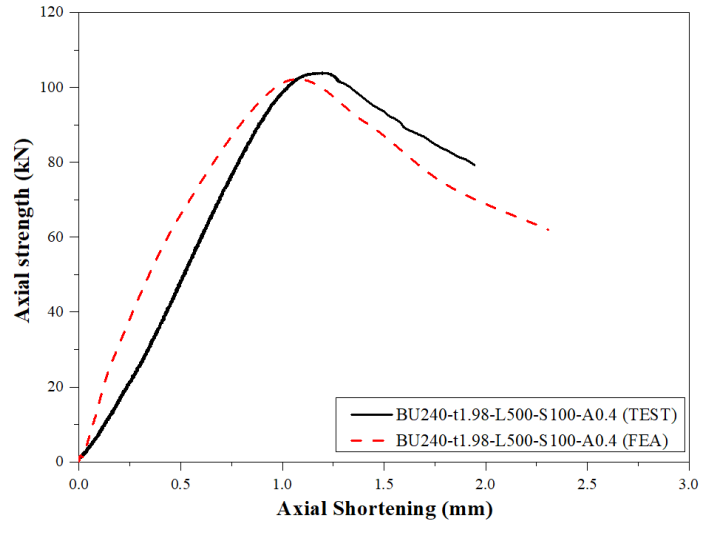

(e) BU240-t1.98-L500-S100-A0.4

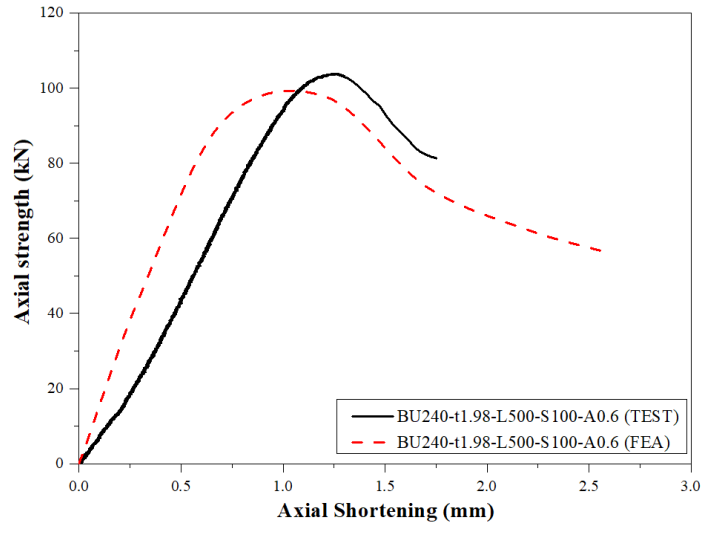

(f) BU240-t1.98-L500-S100-A0.6

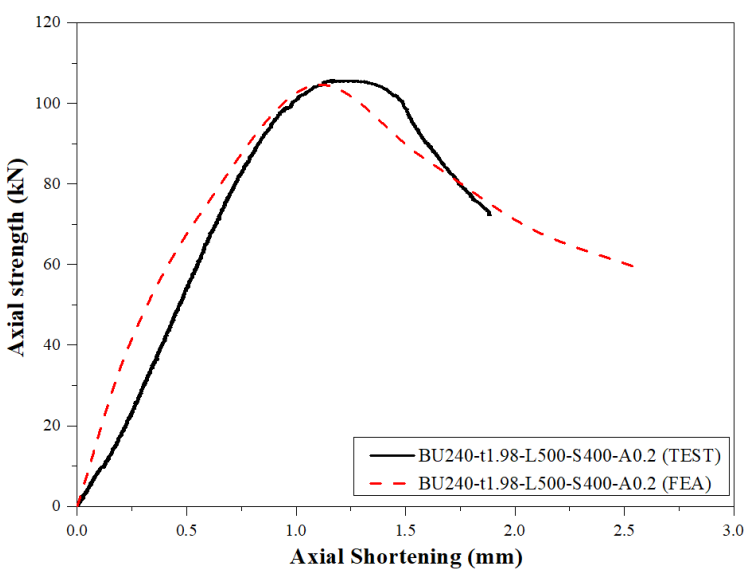

(g) BU240-t1.98-L500-S400-A0.2

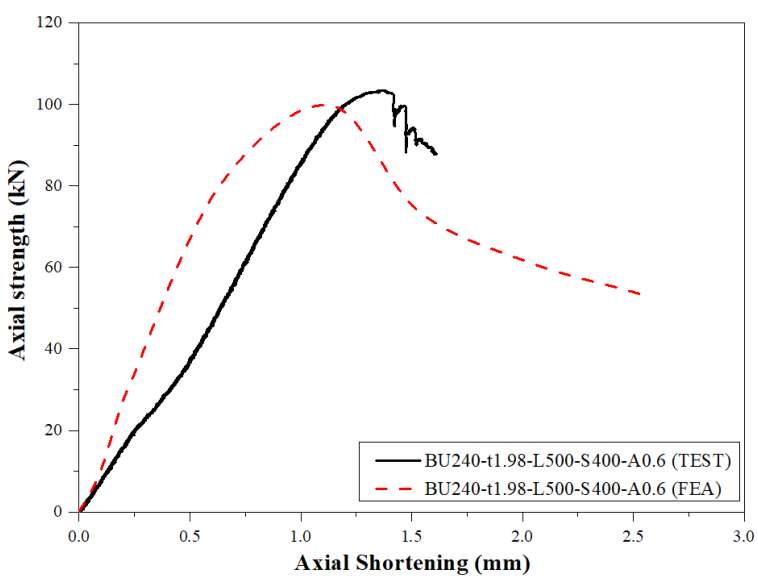

(h) BU240-t1.98-L500-S400-A0.6

Fig.17 Load versus axial-shortening relationship for columns

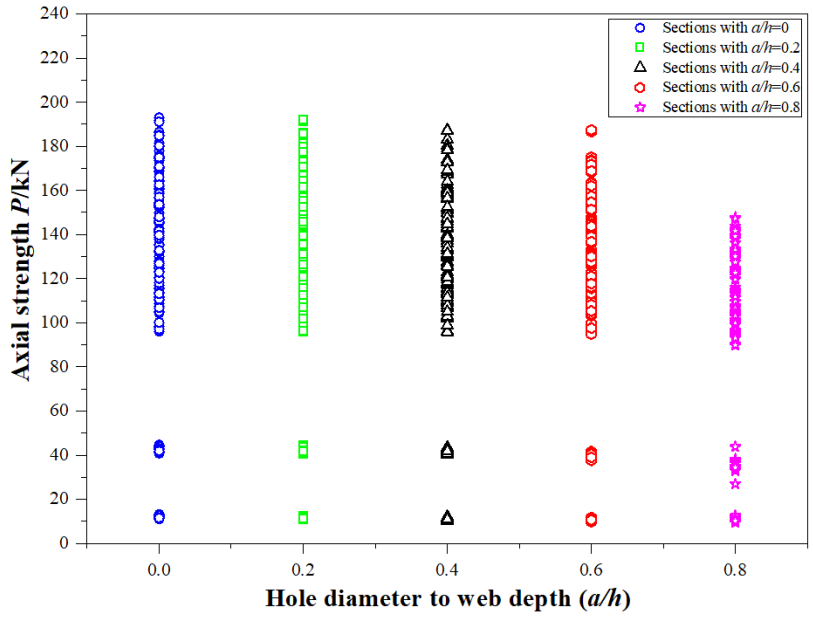

(a) Axial strength of sections against the ratio of *a/h*

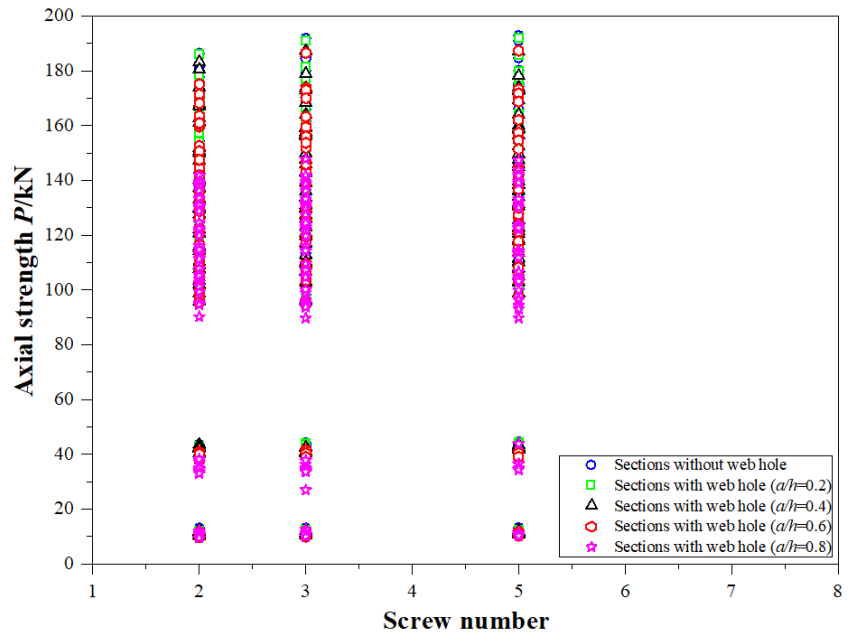

(b) Axial strength of sections against screw number

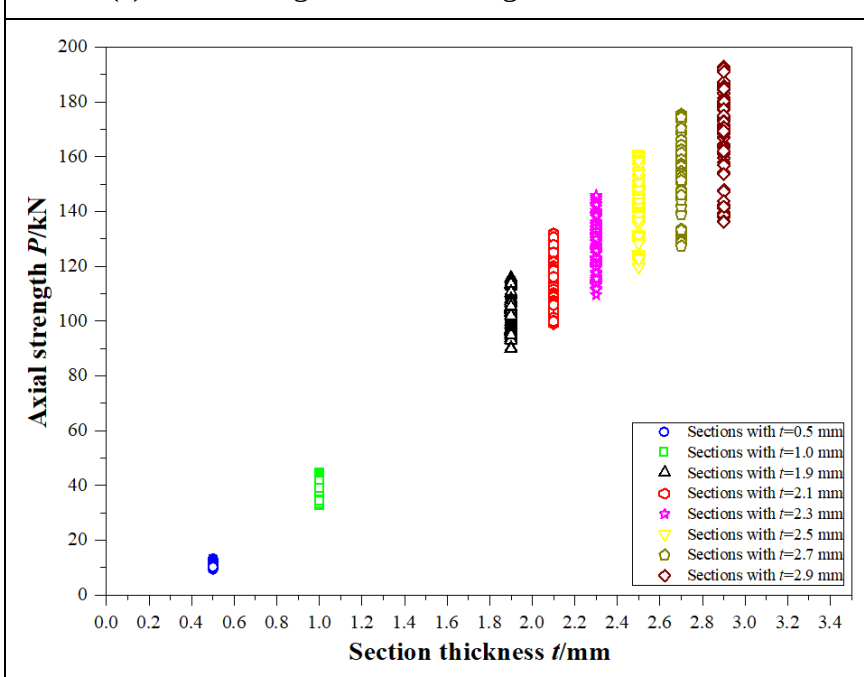

(c) Axial strength of sections against section thickness

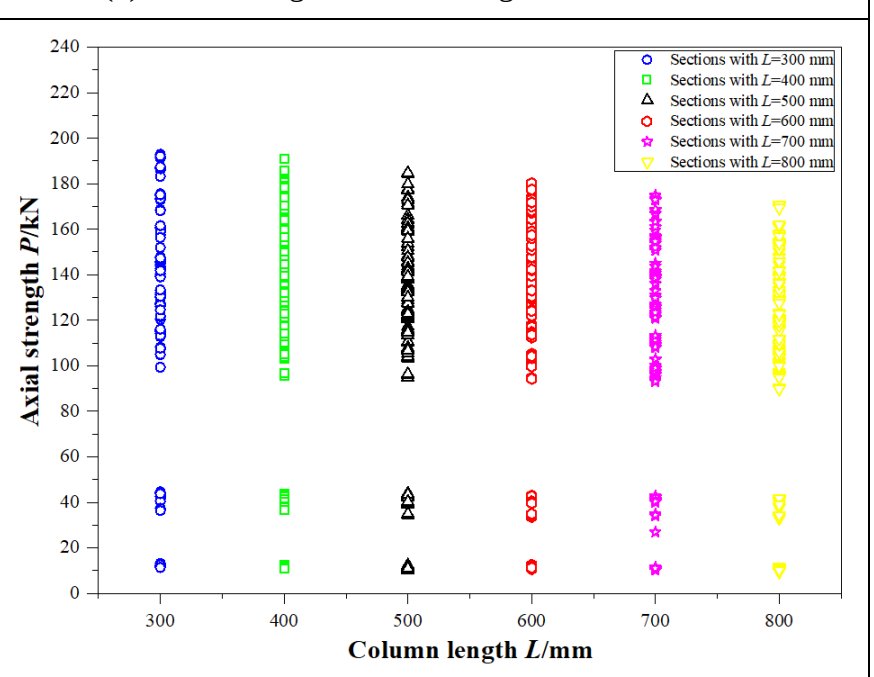

(d) Axial strength of sections against column length

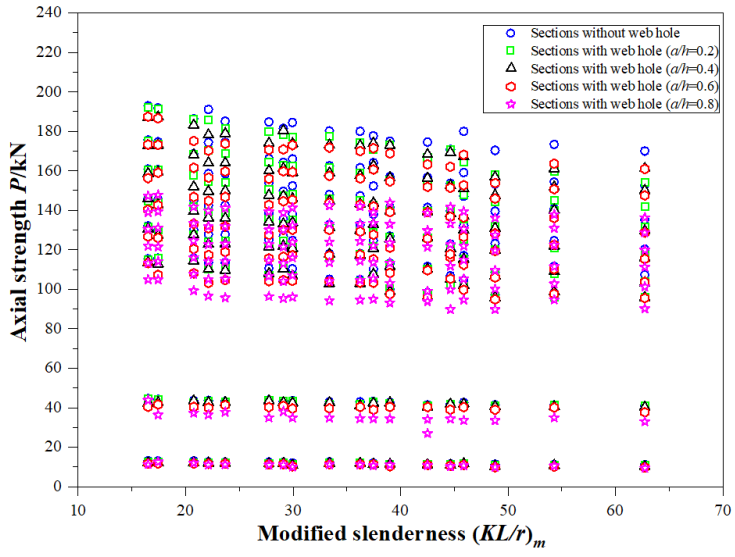

(e) Axial strength of sections against modified slenderness

Fig.18 Parametric effects on axial strength of investigated sections

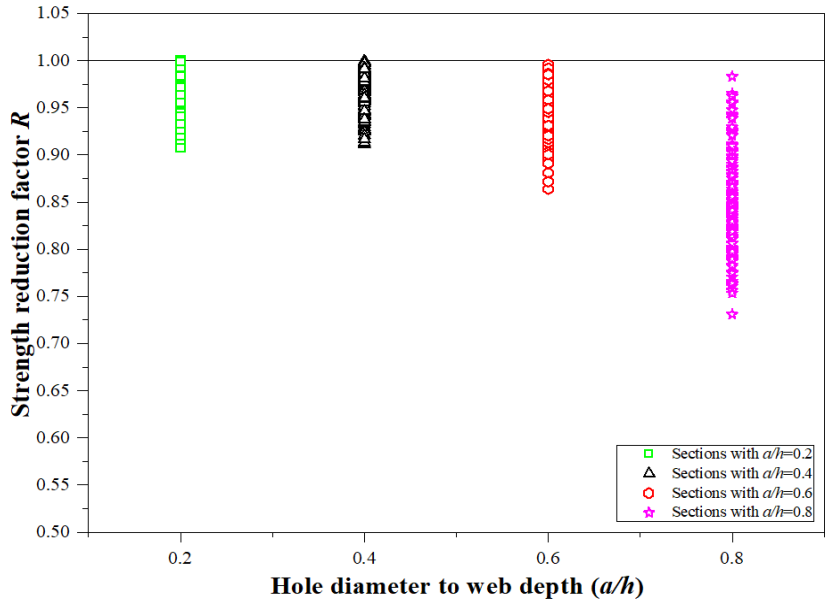

(a) Strength reduction factor of sections against the ratio of *a/h*

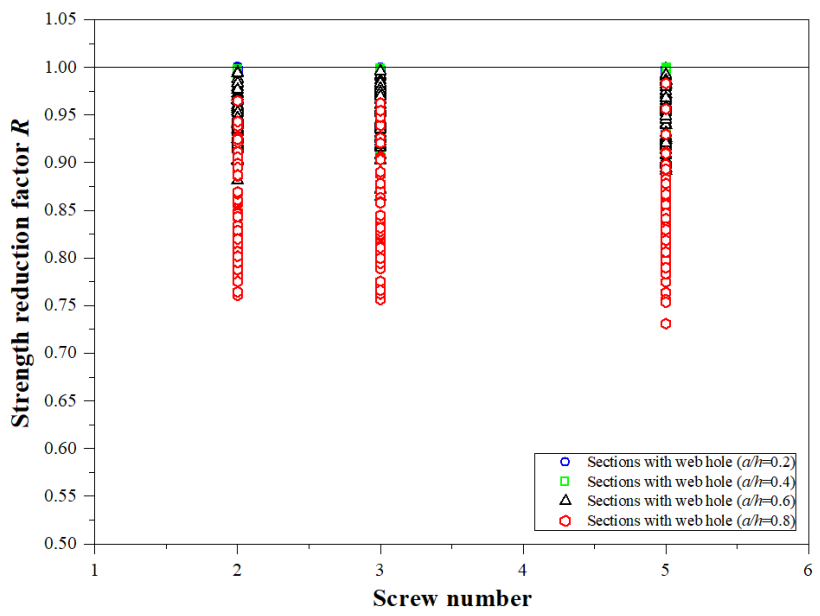

(b) Strength reduction factor of sections against screw number

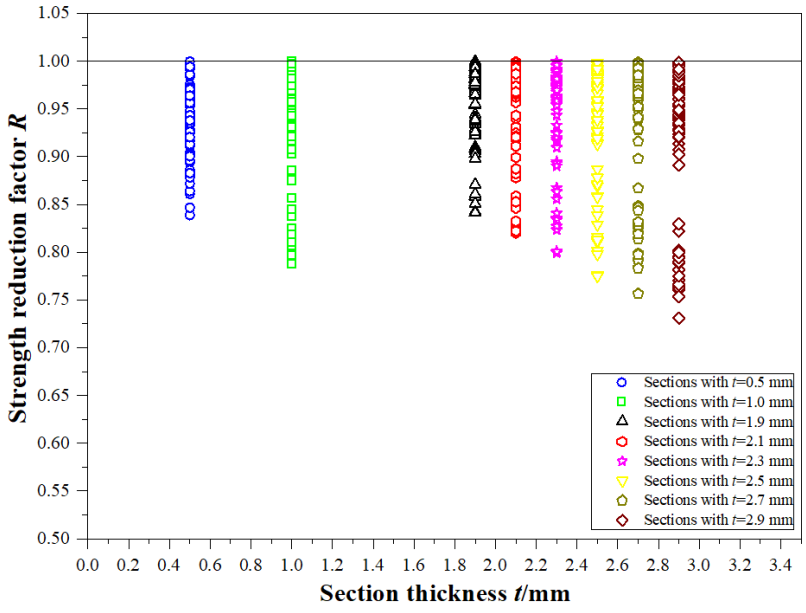

(c) Strength reduction factor of sections against section thickness

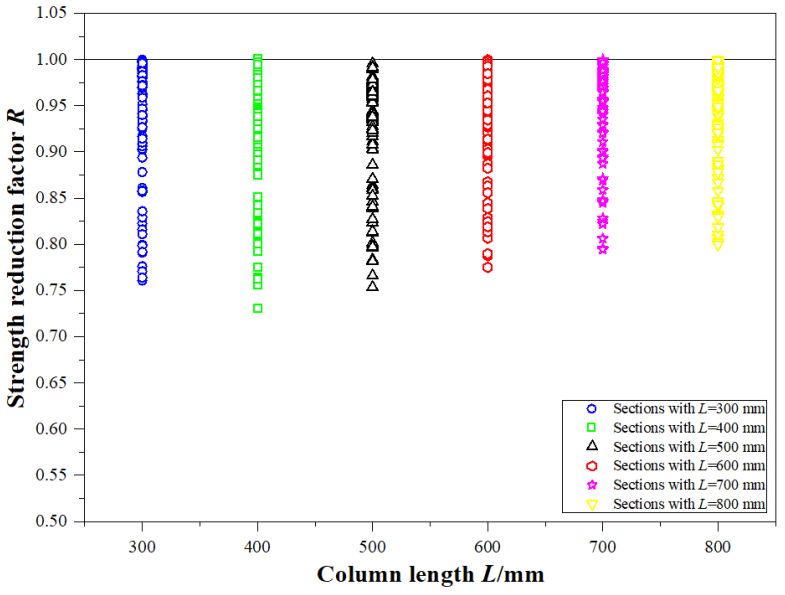

(d) Strength reduction factor of sections against column length

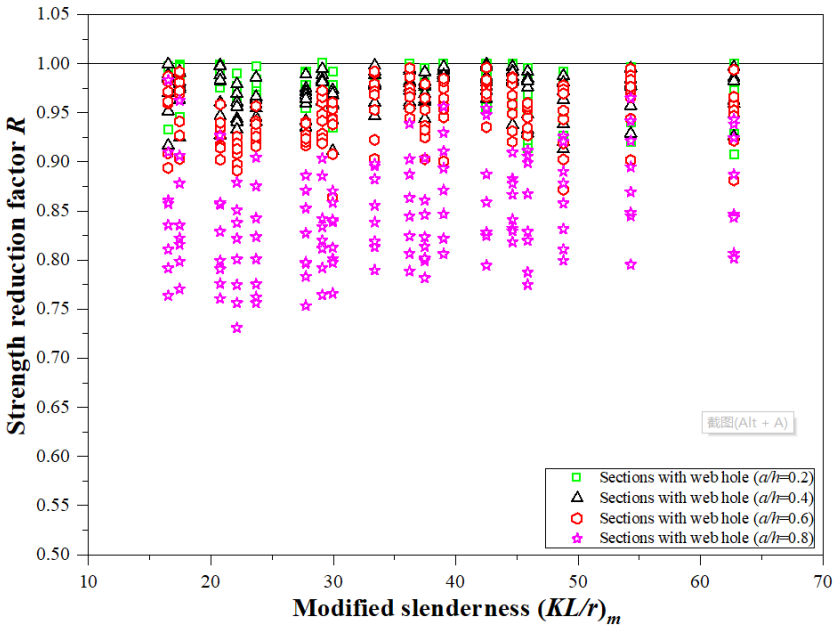

(e) Strength reduction factor of sections against modified slenderness

Fig.19 Parametric effects on axial strength reduction factor of investigated sections

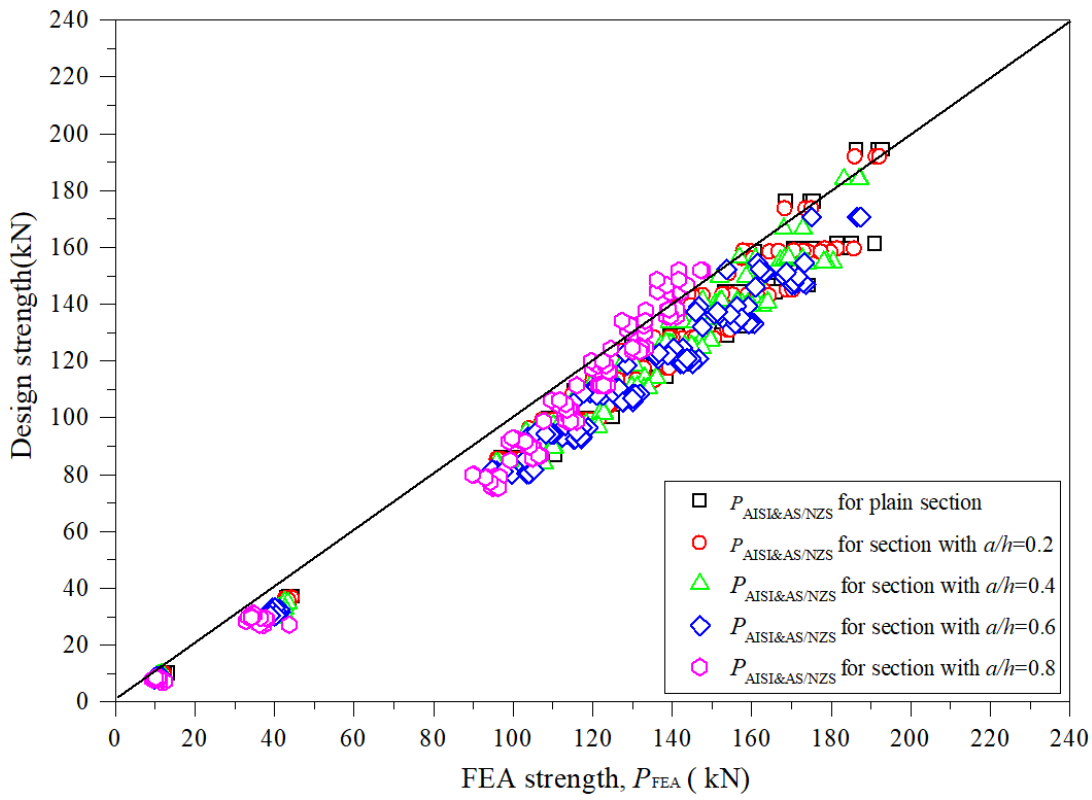

Fig.20 Comparison of axial strengths obtained from the FEA and the current design standards (AISI & AS/NZS)